Recent experiments in quantum optics and their implications – I

Amitabh Joshi[†,*] and Suresh V. Lawande[‡]

[†]Laser and Plasma Technology Division, Bhabha Atomic Research Centre, Trombay, Mumbai 400 085, India
[‡]Department of Physics, University of Pune, Pune 411 007, India

We discuss novel quantum effects pertaining to single atoms and/or photons in the recently developed state-of-the-art experiments with ion traps and microwave/optical cavities cooled to very low temperatures. These experiments are important from the point of view of fundamental physics as well as due to the growing field of quantum information/computation. In the first part of the article, we mainly concentrate on the experiments in ion traps such as observation of quantum jumps along with the underlying theory. We have also discussed non-classical nature of light, quantum Zeno effect and interaction free measurement.

A single atom, nearly at rest in an empty universe, for arbitrary long periods of time, is an ideal quantum system for experiments to test some of the intriguing fundamental aspects of physics. Experiments in such systems have now become possible because of two major advances. The first is the development of tunable lasers in the early seventies which has allowed manipulation of atomic motion in many ways. This has led to several proven schemes of cooling and trapping of atoms and ions in the electromagnetic field. The second is the development of the superconducting cavities with very high quality factors ($Q \approx 10^9 - 10^{10}$).

The major motivation for carrying out experiments with single atom, has been to study pure quantum effects. These experiments have been carried out with a single atomic ion stored in an ion trap or with neutral atoms in a microwave or an optical cavity. Recent experiments on single atomic ions confined in electromagnetic traps have demonstrated some fundamental aspects of physics related to quantum mechanics. Some of these are photon antibunching, squeezing, quantum jumps, quantum Zeno effects, etc. Photon antibunching and quantum jumps are related to the physical manifestations of an atom's abrupt transition between energy states. The quantum Zeno effect refers to the inhibition of transition between quantum states by frequent measurements.

The other class of experiments involves interaction of a single Rydberg atom with a single mode of the electromagnetic field in high-Q microwave cavities. The system is known as one-atom maser or micromaser. The corresponding one-atom laser has also been demonstrated in an optical cavity recently. These experiments in cavities have figured out very subtle effects like the collapse and revival in the Rabi nutation and vacuum Rabi-field oscillation.

The importance of these experiments stems from the observation of the rate of technological progress, also known as the Moore's law. The law states that the number of transistors per chip (or the complexity of a computer) grows exponentially with time and it doubles every year. This law has been obeyed almost precisely over the last thirty years. If this exponential growth is extrapolated into the near future, we foresee that at Moore's rate, a bit of information will be encoded into a single atom by the year 2017. In fact, even before that, quantum effects will be important for computation purposes and an entirely new process of computation known as *quantum computation* will be dominating the technological scenario. Both ion traps as well as cavity quantum electrodynamics experiments will be at the heart of quantum computation.

This article is divided into two parts. The first part will cover the basic schemes of the single atom/ion experiments in ion traps and their interpretations. Current status and probable future directions will be presented.

Non-classical features of light

The advent of lasers in the early sixties prompted an examination of non-classical features of light. Closely connected with this issue is the ubiquitous phenomenon of spontaneous emission. This led to the study of resonance fluorescence problem of spontaneous emission in an applied coherent field. Another important aspect of the spontaneous emission involves the influence of mirrors and cavities on the radiative properties of the atom.

It was soon realized that a beam of light is characterized by the statistical distribution of photons in the beam. The conventional first-order coherence experiments like the Young's double-slit experiment or Michaelson interferometry measure only the 'coherence length' of light by means of fringe contrast. These experiments are in the regime of one photon or linear optics. One needs to

*For correspondence. (e-mail: a_joshi@apsara.barc.ernet.in)

go beyond the experiments of one-photon optics in order to detect any unique quantum mechanical character of light.

The framework for the theory of photon statistics was introduced by Glauber in 1963 (ref. 1). It is based on the intensity–intensity correlation function. For example, a linearly polarized light is characterized by

$$E(\vec{r},t) = E^{-}(\vec{r},t) + E^{+}(\vec{r},t), \tag{1}$$

$$E^{-}(\vec{r},t) = -i\sum_{k}\left(\frac{\hbar\omega_k}{2\varepsilon_0 V}\right)^{1/2} a_k^{\dagger}\exp[i(\omega_k t - \vec{k},\vec{r})], \tag{2}$$

where $E^{+} = (E^{-})^{\dagger}$, V is the quantization volume, ω_k and k are the frequency and the wave vector of a photon and $a_k, a_k^{\dagger}$ are the photon annihilation and creation operators of the kth mode. The quantum mechanical definitions of the mean light intensity $\langle I(E)\rangle$ and the intensity–intensity correlation function of second order $g^{(2)}(\tau)$ are defined as follows

$$\langle I(t)\rangle = \langle E^{(-)}E^{(+)}\rangle, \tag{3}$$

$$g^{(2)}(\tau) = \langle T: I(t)I(t+\tau):\rangle/\langle I(t)\rangle^2$$

$$= \langle E^{(-)}(t)E^{(-)}(t+\tau)E^{(+)}(t+\tau)E^{(+)}(t)\rangle/\langle E^{(-)}(t)E^{(+)}(t)\rangle^2. \tag{4}$$

Note that the second-order intensity correlation $g^{(2)}(t)$ implies that both normal ordering and time ordering are normalized. The symbol $\langle . . .\rangle$ denotes the expectation value or the trace taken over the quantum statistical density operator.

Physically, $g^{(2)}(t)$ is the measure of the probability of detecting a photon at time $t + \tau$, given that a photon was detected at time t. An apparatus for intensity correlation measurement was introduced by Hanbury-Brown and Twiss in the early fifties[2]. The principle of the experiment is as shown in Figure 1. Light from a narrow bandwidth source S is collimated by a pinhole and is split by a half-silvered mirror BS. Some light is transmitted to the photodetector PM2 and some reflected to the detector PM1. The outputs from the two photodetectors are correlated by an analogue or a digital correlator C. The coincidence rate in the detection response is plotted against a time delay τ, which is a measure of the intensity correlation.

Photon antibunching

In order to see the relation between second-order intensity correlation function $g^{(2)}(t)$ and photon statistics consider a single-mode light (beam of photons of single frequency) which can be described by the annihilation and creation operators a, $a^{\dagger}$ obeying the commutation rule $[a, a^{\dagger}] = 1$. In this case,

$$g^{(2)}(0) = \langle a^{\dagger}a^{\dagger}aa\rangle/\langle a^{\dagger}a\rangle^2,$$

$$= \langle \hat{n}(\hat{n}-1)\rangle/\langle \hat{n}\rangle^2,$$

$$= 1 + (\sigma^2 - \langle \hat{n}\rangle)/\langle \hat{n}\rangle^2, \tag{5}$$

where $\hat{n} = a^{\dagger}a$ is the photon number operator and $\sigma^2 = \langle \hat{n}^2\rangle - \langle \hat{n}\rangle^2$ is variance of the photon number distribution. The second step in eq. (5) indicates a remarkable fact that an act of quantum measurement destroys a photon from the beam, i.e., when a second measurement is made, there is one photon less in the beam. Also, the expectation value $\langle . . .\rangle$ depends on the state or on the photon number distribution $P(n)$.

As a consequence of Planck's distribution, thermal light obeys the power law distribution[3]

$$P(n) = \frac{\langle \hat{n}\rangle^n}{(1+\langle \hat{n}\rangle^{n+1})}, \quad \langle \hat{n}\rangle = [\exp(h\nu/kT) - 1]^{-1}. \tag{6}$$

This distribution yields $\sigma^2 = \langle \hat{n}\rangle^2 + \langle \hat{n}\rangle$ and hence $g^{(2)}(0) = 2$. A laser beam in the coherent state has a photon number distribution

$$P(n) = \frac{\langle \hat{n}\rangle^n \exp(-\langle \hat{n}\rangle)}{n!}, \tag{7}$$

leading to $\sigma^2 = \langle \hat{n}\rangle$ and hence $g^{(2)}(0) = 1$. Clearly, light with sub-Poissonian distribution has $g^{(2)}(0) < 1$. The simplest example of this is a number state for which $\sigma^2 = 0$, $\langle n\rangle = n$, yielding

$$g^{(2)}(0) = 1 - \frac{1}{n} \quad n \geq 2,$$

$$= 0 \qquad n < 2. \tag{8}$$

This example also shows that antibunched light (in which photons avoid to come in pairs and thus show anti-correlation) can be described only quantum mechanically.

Resonance fluorescence

First evidence of antibunching and quantum jumps was provided by the simple phenomenon of resonance fluorescence from a two-level atom of transition frequency ω_0 which is continuously driven by a near resonant laser of frequency ω (Figure 2). Typically, ω_0 and ω are in the optical region (10^{11}–10^{15} Hz). The Rabi frequency 2Ω

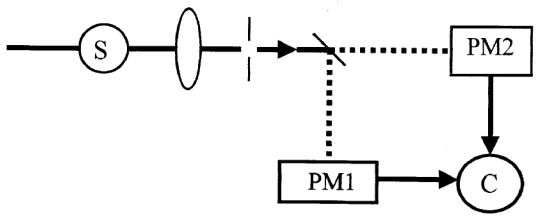

Figure 1. Schematic diagram of the Hanbury-Brown and Twiss apparatus used for measuring second-order intensity–intensity correlation.

($\Omega = (d \cdot E)/2\hbar$, where d is the induced dipole moment and E is laser field amplitude) is around a few GHz corresponding to a laser power of a few mW. The spontaneous emission of a photon from the excited atom is characterized by the Einstein A coefficient also called γ. The mean lifetime A^{-1} or γ^{-1} of the upper level may vary from 10^{-6} to 10^{-9} s. If the field is intense ($\Omega \gg \gamma$), the atom will be excited and de-excited several times, giving rise to Rabi oscillations. The spontaneous emission damps out the oscillations and the atomic observables like the mean population difference or the mean polarization will attain their steady-state value eventually.

What is of particular interest is the fluorescence or the photons that are scattered by the atom. These photons will be emitted in all directions (i.e. in 4π solid angle) and in an experiment it is necessary, to monitor them in a direction transverse to that of the incident laser beam and the atomic beam in order to avoid mixing with the pump photons.

The intensity correlation function $g^{(2)}(\tau)$ for resonance fluorescence from a two-level atom is given by[4,5]

$$g^{(2)}(\tau) = (1 - e^{-\gamma\tau})^2, \quad \Omega \ll \gamma;$$
$$= (1 - e^{-3\gamma\tau/2} \cos(2\Omega\tau)), \quad \Omega \gg \gamma. \qquad (9)$$

The behaviour of $g^2(\tau)$ for $\Omega \ll \gamma$ and for $\Omega \gg \gamma$ is shown by curves (i) and (ii) in Figure 3. For small fields ($\Omega \ll \gamma$), $g^{(2)}(\tau)$ shows a steady increase from its value $g^{(2)}(0) = 0$ to its final value $g^{(2)}(\infty) = 1$. For intense fields ($\Omega \gg \gamma$), the behaviour is oscillatory, decaying to the value unity. This behaviour is to be compared with $g^{(2)}(\tau)$ for laser (coherent) light source (curve (iii)) and that for thermal light source (curve (iv)). For laser light $g^{(2)}(\tau) = 1$ for all τ, while for thermal light $g^{(2)}(\tau)$ decays from its initial value 2 to its final value 1. Thermal light signifies what is known as photon bunching (photons prefer to arrive at the detector in pairs). In contrast, light with $g^{(2)}(\tau) < 1$ shows anti-correlation or antibunching. $g^{(2)}(\tau) = 1$ implies statistical independence between the light incident on the two photodetectors in the intensity correlation experiment discussed earlier (Figure 1). This is the case for coherent light.

In contrast, the intensity correlation for thermal light is

$$g^{(2)}(\tau) = 1 + e^{-\gamma^2\tau^2}. \qquad (10)$$

This is known as the Hanbury-Brown and Twiss (HBT) effect, where γ is the spectral width. The coincidence rate at zero delay time τ is twice as large as that in the steady state at large τ (see curve (iv), Figure 3).

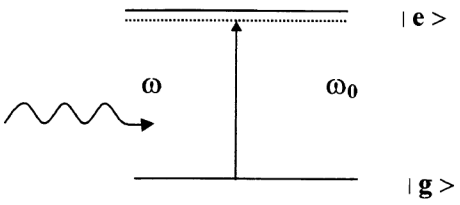

Figure 2. Two-level atom interacting with a coherent field of laser.

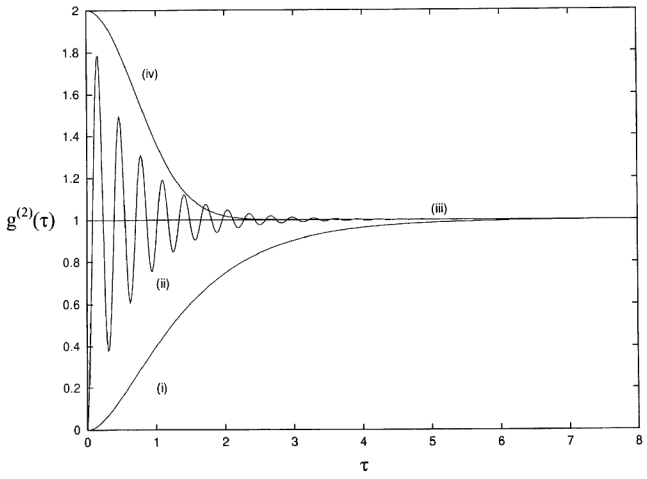

Figure 3. Second-order intensity–intensity correlation function (theoretical) vs as a function of τ. Curves (i) and (ii) are for the fluorescence light, while curves (iii) and (iv) are for laser and thermal light, respectively.

Experimental observation of antibunching

Experiments on observation of antibunching in resonance fluorescence were first carried out by Kimble, Dagenais and Mandel[6] on sodium atoms undergoing a transition $3^2S_{1/2} \rightarrow 3^2P_{3/2}$. Briefly, atoms of sodium in a dilute atomic beam (on the average one atom in the interaction zone) are excited by the light beam of a tunable dye laser (Figure 4) stabilized in intensity to a few per cent and in frequency to about 1 MHz. The laser is tuned to the ($3^2S_{1/2}$, $F = 2$) to ($3^2P_{3/2}$, $F = 3$) transition. By optically prepumping with circularly polarized light in a weak magnetic field (4–5 Gauss) before the final interaction, the sodium atoms are prepared in the $3^2S_{1/2}$, $F = 2$, $m_F = 2$ state. Such a procedure devised by Abate[7] assures that

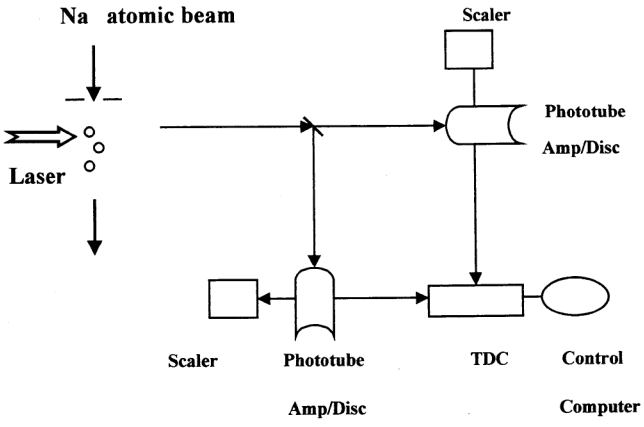

Figure 4. Schematic diagram of apparatus employed in experimental investigation of antibunching.

the atoms behave like a two-level quantum system. The resonant optical field seen by such atoms has a power density of about 70 mW/cm^2 ($\Omega/\gamma = 4$–5). The fluorescent light emitted is collected at right angles to both the laser and the atomic beams by means of a microscope objective and subjected to photon correlation measurements using HBT apparatus. The results were in agreement with theory described here after appropriate corrections for transit time broadening and multi-atom effects were accounted for. Physically, the vanishing of $g^{(2)}(\tau)$ at $\tau = 0$ for a single atom implies that the excited atom having emitted a photon at time t is unable to radiate again immediately after having made a quantum jump back to the lower state. From the point of view of quantum measurement theory, although the state of an excited state evolves continuously in absence of observation, there is sudden return to the lower state when a photon is detected.

More recently, the application of a radio frequency (RF) trap to study the resonance fluorescence of a single, stored $^{24}Mg^+$ ion has been demonstrated by Diedrich and Walther[8]. Figure 5 shows two types of ion traps, Penning trap and Paul (RF) trap, that are commonly used for spectroscopic experiments (the difference between the two has been explained in the caption of Figure 5). The transition used was $3^2S_{1/2} \rightarrow 3^2P_{3/2}$, ($\lambda = 2800$ Å). In the experiments, the ion is stored in a Paul (RF) trap mounted inside a stainless steel ultrahigh vacuum chamber. At a pressure of 5×10^{-11} mb, the ion can be stored for about 10 min. The single ion is closely confined in the centre of the trap by photon recoil cooling. The large size of the trap permitted a large solid angle for the detection of the fluorescence radiation.

The intensity correlations of the fluorescence light were investigated by means of an ordinary HBT set-up with two photomultipliers and a beam splitter. The intensity correlation function $g^{(2)}(\tau)$ could thus be checked. The photon correlation signals show the non-classical

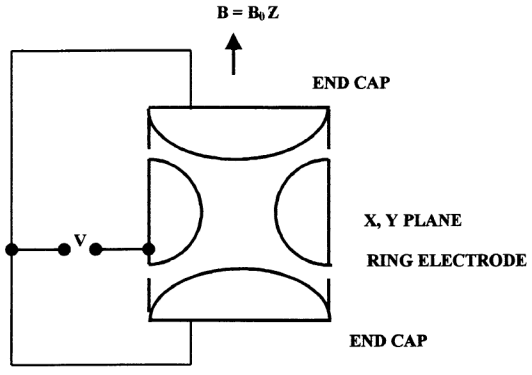

Figure 5. Schematic diagram of Penning/Paul (RF) trap. For the Penning trap, magnetic field B is required but sinusoidal field to the ring electrode is not required, e.g. $V = V_0 + v_m \cos(\omega t)$ (ω is the frequency of the RF field) and $v_m = 0$ for the Penning trap.

antibunching effect connected with Rabi oscillations, which are damped out during the excited state lifetime, but a periodic feature resulting from the oscillation of the ion in the trap survives.

Another interesting aspect of this experiment was that sub-Poissonian statistics which is associated with antibunching property in resonance fluorescence could also be measured. Short and Mandel[9] had earlier measured this for sodium atoms using the dilute atomic beam and a special trigger scheme for a single atom event. In the experiment by Diedrich and Walther's, the sub-Poissonian character was inferred by determining the number of events ΔN in which two photons arrive within the time interval ΔT. During a running time $T = 1252$ s a total number of 5.9×10^7 photons were detected, which gives for $\Delta T = 4.607$ ns, $\Delta N = 3200$ events according to Poissonian statistics. Instead 1583 events were counted, a result that differs by 28 standard deviations from Poissonian statistics. The normally ordered variance Q_M (Mandel parameter) gave a value $= -7.0 \times 10^{-5}$, which is smaller than that achieved by Short and Mandel because of the smaller overall detection efficiency of about 4×10^{-4}. Note that $Q_M = (\sigma^2 - \langle \hat{n} \rangle / \langle \hat{n} \rangle < 0$ for sub-Poissonian statistics.

Squeezed light

Squeezed states of electromagnetic field are those showing non-classical behaviour and have no representation in terms of classical (vector) fields, stochastic or otherwise[10]. During investigation of generalized minimum uncertainty state, the idea of squeezed state took shape[10]. Quantum noise (or fluctuations) is the fundamental property of any system and it is present in all kinds of electromagnetic field states, including the field vacuum state. The basic idea of squeezing is the reduction of quantum fluctuations in the quadrature component within the Heisenberg's uncertainty principle. In a coherent state, the fluctuations in the quadrature components are equal and their product is the minimum uncertainty product given by Heisenberg's uncertainty relation. Actually, the quantum fluctuations of a coherent state are zero point fluctuations and are randomly distributed in phase. On the other hand, it is possible to have minimum uncertainty states having reduced fluctuations in one quadrature phase than a coherent state at the expense of increased fluctuations in the other quadrature phase. These states are called squeezed states (which are sometimes referred as two-photon coherent state, generalized coherent states, etc.) in which the quantum noise is not randomly distributed in phase[10].

We illustrate our above discussion with reference to a single-mode field for the sake of simplicity. The expression for the single-mode field of frequency ω is

$$E(t) = \alpha(ae^{-i\omega t} + a^\dagger e^{i\omega t}), \quad (11)$$

where α is a constant containing spatial variation and a, $a^\dagger$ are the annihilation and creation operators for the electromagnetic field obeying Boson commutation relations. It is convenient to write $a = q_1 + iq_2$ such that q_1 and q_2 are Hermitian operators obeying the relation $[q_1, q_2] = i/2$ and the expression for the electric field becomes

$$E(t) = 2\alpha(q_1 \cos(\omega t) + q_2 \sin(\omega t)). \quad (12)$$

Clearly q_1 and q_2 are the amplitudes of the two quadrature phases of the field. We can define uncertainty in the two quadratures as $\Delta q_i = [V(q_i)]^{1/2}$, $(i = 1, 2)$, in which $V(q_i)$ means variance. It is straightforward to show that

$$\Delta q_1 \Delta q_2 \geq 1/4. \quad (13)$$

The equality sign in eq. (13) above is for the class of minimum uncertainty state (MUS). We have in general, $\Delta q_1 \neq \Delta q_2$; yet, the states could be of MUS category. Such states are called squeezed states with the condition that the normally ordered variance

$$V(q_i) < 1/4 \quad (i = 1 \text{ or } 2). \quad (14)$$

Hence, a squeezed state could be defined as the state in which the quantum fluctuations in one quadrature phase are less than those for a vacuum state. As a result of Heisenberg's uncertainty relation, the quantum fluctuations in the other quadrature component are increased compared to the vacuum field.

Action of the displacement operator $D(\beta)$ on the vacuum state $|0\rangle$ gives rise to a coherent state:

$$|\beta\rangle = D(\beta)|0\rangle, \quad (15)$$

where $D(\beta) = e^{-1/2|\beta|^2} e^{\beta a^\dagger} e^{-\beta^* a}$, β is a complex number.

A squeezed state $|\beta, \xi\rangle$ can be produced by application of squeeze operator $S(\xi)$ on the vacuum state followed by the displacement operator $D(\beta)$

$$|\beta, \xi\rangle = D(\beta)S(\xi)|0\rangle, \quad (16)$$

where $S(\xi) = \exp(\frac{1}{2}\xi^* a^2 - \frac{1}{2}\xi a^{\dagger 2})$, $\xi = re^{i\phi}$.

It should be noted that a coherent state is generated by linear terms in $a(a^\dagger)$ in the exponent of $D(\beta)$ whereas the squeezed state requires quadratic terms in $S(\xi)$. The variances in the squeezed state $|\beta, \xi\rangle$ are given by

$$V(p_1) = \tfrac{1}{4} e^{-2r},$$

$$V(p_2) = \tfrac{1}{4} e^{2r}, \quad (17)$$

where $(p_1 + ip_2) = (q_1 + iq_2)e^{-i\phi/2}$ is rotated complex amplitude and $2\Delta p_1$ and $2\Delta p_2$ are the length of minor and major axes, respectively of the error ellipse. Clearly, the variances $V(p_i)$ are not a function of field amplitudes. So one can observe squeezing for the strong field also, which is in contrast to the photon antibunching which can be observed preferably for low-intensity fields. Hence squeezing could be termed as a macroscopic quantum effect.

It is possible to calculate variance in one quadrature using Glauber–Sudershan P representation. For the single-mode field we can have

$$V(q_1) = \tfrac{1}{4}(1 + \int P(\beta)[(\beta + \beta^*) - (\langle\beta\rangle + \langle\beta^*\rangle)]^2 \, d^2\beta). \quad (18)$$

For the squeezed field we require $V(q_1) < 1/4$, which implies $P(\beta)$ to be a nonpositive definite function. But the classical averaging procedure demands $P(\beta)$ to exist as a positive nonsingular function. In this sense, we can regard squeezing like photon antibunching as a non-classical feature of the electromagnetic field state.

The phase space representation of the single-mode coherent field and the squeezed field is shown in Figure 6. The field state is represented by a dot surrounded by a circle (for coherent state) or an ellipse (for squeezed state). The circle or ellipse represents the noise distribution for these states. The coherent (squeezed) state has isotropic (non-isotropic) noise distribution.

The production of a squeezed state from a single-mode field requires mixing of this field with its phase conjugate part, i.e.

$$b = xa + ya^\dagger, \quad (19)$$

and $x^2 - y^2 = 1$. Suppose a represents the field mode in the coherent state, then b represents the field mode in the squeezed state. The phase conjugation can be achieved by a non-linear interaction such as four-wave mixing. The model Hamiltonian describing nonlinear interaction can be written as

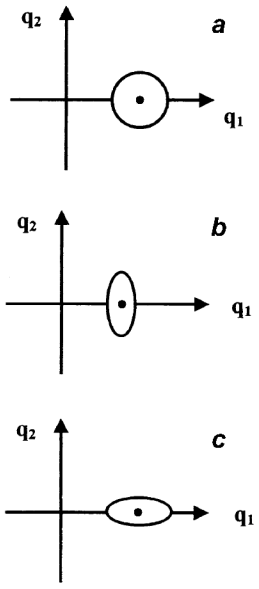

Figure 6. Phase plot of (***a***) coherent state (β real, $\xi = 0$) with the circle representing isotropic noise distribution, (***b***) squeezed state $|\beta, \xi\rangle$ with reduced phase fluctuations (β real, $r > 0$), and (***c***) squeezed state $|\beta, \xi\rangle$ with reduced phase fluctuations (β real, $r < 0$). Ellipse represents noise distribution in (***b***) and (***c***).

$$H_{\text{int}} = \chi_n^* a^2 + \chi_n a^{\dagger 2}, \quad (20)$$

where χ_n represents nonlinear susceptibility of the medium. The first experimental observation of squeezed light was reported in the four-wave mixing experiment[10]. Later, a number of schemes generating squeezed light were studied[10]. The most prominent study utilizes parametric oscillator or a parametric down-converter for generating squeezed light[10].

The squeezed field produced from a parametric oscillator is characterized by a photon number function and two-photon correlation function which are very useful in describing the spectroscopic features of an atom in the squeezed field.

Squeezing is a phase-sensitive phenomenon, as the variances of quadrature field components are different and can be characterized by their phases. So, it becomes mandatory to use phase-sensitive techniques such as homodyning to detect the squeezed field. In this technique, the signal field consisting of squeezed light is homodyned with a local oscillator field (supposed to be in a coherent state). In the limiting condition, when the amplitude of the local oscillator greatly exceeds the signal field, then the photon statistics of the combined field is directly proportional to the variance of the signal field. Thus photon statistics measurement is carried out by changing the local oscillator field phase θ. The change in photon statistics from sub- to super-Poissonian statistics as θ is varied, definitely indicates the presence of squeezing in the signal.

Squeezed light provides a test-bed for fundamental issues related to quantum measurement theory. Possible applications of the squeezed light are in optical communication system, interferometric techniques to detect very weak forces such as gravitational wave detection, optical wave-guide tap and atomic spectroscopy. However, difficulties in obtaining practical squeezed light sources have hampered these applications.

The radiative properties of atoms are very sensitive to their coupling to the environment or the vacuum reservoir. If a normal vacuum reservoir is replaced with a squeezed one, then it has been predicted that the line width of both emission and absorption spectra can be substantially reduced, which could be used in improving resolution in laser spectroscopy of atoms. The intrinsically non-classical features of squeezed light are manifested in various unusual spectral features that have been reported in the literature over the past two decades[10,11].

Quantum jumps in a three-level atom

Basic scheme for observation of quantum jumps

As early as 1975, Dehmelt[12], one of the pioneers in development of ion traps, proposed a scheme to detect a weak (dipole-forbidden) transition in single-atom optical double-resonance spectroscopy. The concept is based on bringing an isolated ion nearly to rest by localizing it in an ion trap and by optically cooling it.

Consider, for example, the three-level ion of Figure 7 *a* with two transitions starting from the common ground state $|3\rangle$. The blue transition $|3\rangle \rightarrow |1\rangle$ is very strong, while the red transition $|3\rangle \rightarrow |2\rangle$ is very weak. The lifetimes $\tau_1(\gamma_1^{-1})$ and $\tau_2(\gamma_2^{-1})$ of the levels $|1\rangle$ and $|2\rangle$ are, for example, of the order of 10 ns and 1 s, respectively. The narrow, weakly allowed transition is detected as follows. The ion is assumed to be in the ground state $|3\rangle$ initially. The light at the wavelength near the transition $|3\rangle \rightarrow |2\rangle$ is pulsed on, possibly driving the ion to the level $|2\rangle$. Light at a wavelength near the blue transition $|3\rangle \rightarrow |1\rangle$ is then pulsed on. If the ion had made a transition in the previous step, no fluorescence (γ_1) would be observed: otherwise an easily detectable fluorescence signal would be observed. This method is called 'electron shelving', since the optically active electron is temporally shelved on the upper level $|2\rangle$ of the weak transition. Also, because the weak transition line width may be extremely narrow, this scheme has been proposed as an ultimate laser frequency standard, perhaps with a resolution of 1 part in 10^{18} ($\Delta\nu/\nu \approx 10^{-18}$).

The electron shelving technique as a means of direct observation of quantum jumps was first pointed out by Cook and Kimble[13]. Suppose two lasers (with wavelengths near the two transitions) drive the two transitions continuously. Since the blue transition is strong, most of the time due to spontaneous emission from level $|1\rangle$ fluorescence is seen. But the moment the ion absorbs a red photon it is shelved in $|2\rangle$ and the fluorescence is extinguished. When the 'shelved ion' returns to the ground state $|3\rangle$ either by spontaneous or stimulated emission, it triggers a succession of blue photons in the strong transition, resulting in an amplification by a factor

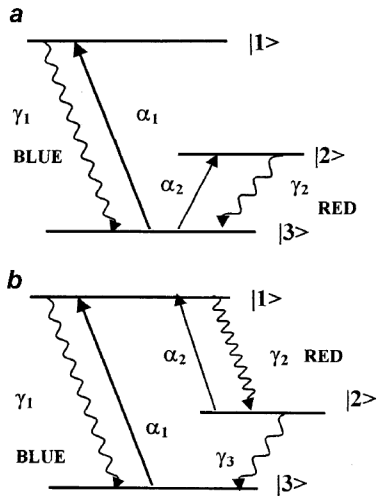

Figure 7. Scheme for observation of quantum jumps. ***a***, V-system with $\tau_1 = 1/\gamma_1 = 10$ ns, $\tau_2 = 1/\gamma_2 = 1$ s; ***b***, Same for Λ or Raman-system.

$\approx \tau_2/\tau_1 \approx 10^8$. Thus the fluorescence observed on the strong transition should turn off and on abruptly, as the ion makes transitions to and from the metastable state. Also, since the weak transition occurs randomly in time, the atomic fluorescence $I(t)$ (photons/s) has the form of a random telegraph signal shown in Figure 8. Incidentally, the jumps in the level configuration of Figure 7 *a* are known as jumps on absorption. In the alternative scheme shown in Figure 7 *b*, the shelf level $|2\rangle$ is coupled to the excited level $|1\rangle$. Raman scattering from level $|1\rangle$ shelves the ion in the metastable level $|2\rangle$ from which it decays to the ground state $|3\rangle$. Jumps in this scheme are known as the jumps on emission. Note that the transitions $|1\rangle \rightarrow |2\rangle$ and $|2\rangle \rightarrow |3\rangle$ are both very weak. This scheme is nowadays experimentally popular, because only one laser driving the strong transition $|3\rangle \rightarrow |1\rangle$ is required. However, the jumps in this scheme may be controlled by applying a second field driving the transition $|2\rangle \rightarrow |1\rangle$.

For the scheme shown in Figure 7 *a*, Cook and Kimble[13] investigated theoretically, the dynamics of the process using rate equations by assuming the driving fields to be incoherent along with a complete saturation of the strong transition. The analysis resulted in a simple expression for transition rates between the weakly coupled state and the pair of strongly driven states. These rates correspond to the switching on and off of the fluorescence on the strong transition, resulting in a simple picture of a random telegraph. Further, it was predicted that both the darkness and brightness intervals are distributed exponentially.

Experiments on quantum jumps

Subsequent to the theoretical analysis of Cook and Kimble[13], several experimental observations on quantum jumps have been reported. The first experiment by Nagourney *et al.*[14] at the University of Washington, was on Ba^+ ion trapped in a miniature RF (Paul) trap with the level structure shown in Figure 9 *a*. The ion is cooled ($T < 10$ mK) and localized to < 1 μm by simultaneous irradiation from the continuous wave (cw) light of two dye lasers driving the transitions $6^2S_{1/2} \rightarrow 6^2P_{1/2}$, ($\lambda_1 = 493$ nm) and $5^2D_{3/2} \rightarrow 6^2P_{1/2}$, ($\lambda_2 = 650$ nm). The red light serves to re-excite the ion when it has decayed to the metastable $5^2D_{3/2}$ state. The shelf level is $5^2D_{5/2}$ with lifetime around 47 ns. Coupling to this level is achieved by means of an incoherent excitation to $6^2P_{3/2}$ level from a Ba-hollow cathode lamp and a subsequent decay to $5^2D_{5/2}$. In other words, to observe quantum jumps it is necessary to transfer the ion into $5^2D_{5/2}$ level. The blue-green fluorescence is monitored ($6^2P_{1/2} \rightarrow 6^2S_{1/2}$), which shows a sudden quenching whenever the ion jumps to the metastable level $5^2D_{5/2}$ and a switching on when the ion decays back to the ground state. A second experiment by Sauter *et al.*[15] at Hamburg University on Ba^+ used trapping of the ion in the shelf-level ($5^2D_{5/2}$) by incoherent Raman scattering from the excited level $6^2P_{1/2}$ (Figure 9 *b*). Here also, the resonance fluorescence ($6^2P_{1/2} \rightarrow 6^2S_{1/2}$) is monitored and it vanishes whenever there is a transition occurring to metastable $5^2D_{5/2}$ level via incoherent Raman scattering and reappears when the metastable level decays back to the $6^2S_{1/2}$ level.

A series of experiments were carried out by Wineland's group[16,17] at NBS Boulder on trapped Hg^+ ion, in which there is a strong resonance transition from the $5d^16s^2S_{1/2}$ ground state to $5d^16s^2P_{1/2}$ state near 194 nm. The lifetime of the $^2P_{1/2}$ state is around 2–3 ns. There is a 'weak' electric quadrupole transition from the $^2S_{1/2}$ ground state to $5d^96s^2\ ^2D_{5/2}$ state near 282 nm (lifetime ≈ 0.1 s). In addition to its usual decay to the ground state by electric dipole (E_1) radiation, the $^2P_{1/2}$ has a small probability of undergoing E_1 decay to the metastable $^2D_{3/2}$ level. From the $^2D_{3/2}$ level, the ion decays directly to

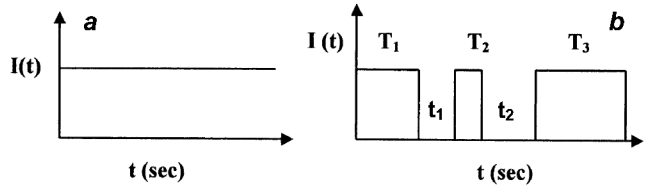

Figure 8. Fluorescence intensity $I(t)$ as a function of time t. ***a***, Behaviour of $I(t)$ when the 'red' laser is off; ***b***, Intermittent blue fluorescence when both lasers are on. The length of brightness (T_i) and darkness (t_i) intervals is randomly distributed.

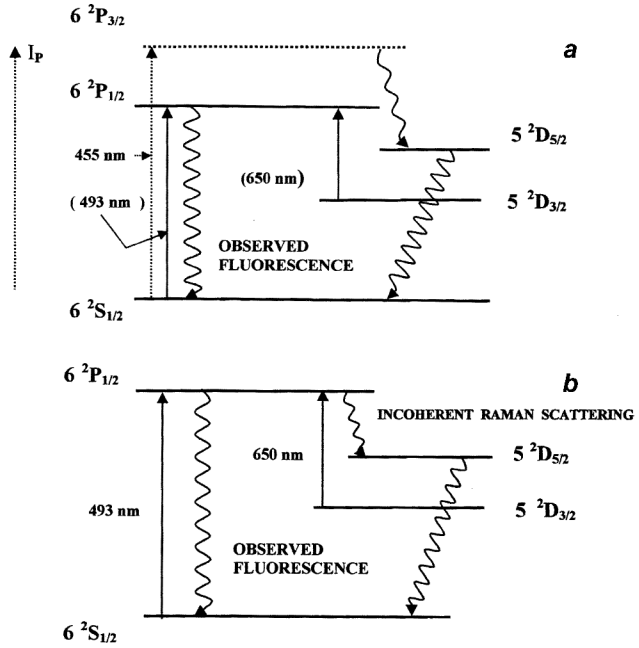

Figure 9. Level structure of Ba^+ ion quantum jump measurements. Transition $^2S_{1/2} \rightarrow {}^2P_{1/2}$ is strong. Shelf level is $^2D_{5/2}$. ***a***, Incoherent pumping from $^2S_{1/2} \rightarrow {}^2P_{3/2}$ followed by decay shelves the ion in level $^2D_{5/2}$. Blue-green fluorescence so monitored on $6^2P_{1/2} - 6^2S_{1/2}$ changes randomly. The ion trapped in level $5^2D_{5/2}$ eventually decays down to ground level spontaneously. ***b***, Shelving of ions in $^2D_{5/2}$ level is due to incoherent Raman scattering from the level $6^2P_{1/2}$.

Box 1.

Magnetic traps

Magnetic traps are based on the utilization of magnetic moment of atoms for their trapping with the help of an external magnetic field. Atoms with unpaired electrons, e.g. all alkali atoms, have finite magnetic moment and they respond to the external magnetic field by aligning their magnetic moments either parallel or antiparallel to the direction of the magnetic field. This gives a Zeeman shift to the atom's energy. When the applied magnetic field is non-uniform and has spatial gradient, the response of the atom is decided by the nature of the magnetic moment. If the atoms have positive magnetic moment, they will start moving towards the direction where the magnetic field strength is maximum, but for the negative magnetic moment, the atoms move towards minimum magnetic field and can be thus trapped. Alternatively, atoms with negative Zeeman shift move towards highest magnetic field region and those with positive Zeeman shift move to the region of lowest field and are trapped. Such a device is called a magnetic trap.

Optical traps

Magnetic traps are quite good, but there is difficulty in control. To have better control, optical trapping is employed which is based on the induced electric dipole moment of the atom. The origin of dipole moment can be explained by considering the atom to be a polarizable body. A laser beam detuned in frequency from the resonance transition frequency of the atom will control the random photon emission and the dipole moment so induced in the atom will interact with the electric field of the laser beam and constitute a force along the gradient of the intensity. The direction of this force is decided by the nature of detuning. The electric polarizability is positive below the resonance and negative above the resonance. If the laser frequency is below the atomic resonance frequency, force will be directed in the region towards larger laser intensity and thus atoms move in the region of higher intensity and can be trapped. Alternatively, it can be understood as follows: For red detuning, there is a potential well for the ground state and atoms are attracted into the region of high intensity. Such a trapping mechanism is used in optical traps. The characteristic feature of such traps is that if the laser beam is moved then the trapped atoms follow, such that the cold atoms can be moved from place to place. This kind of manipulation using optical tweezers is also possible for bacteria or living cells in water (Ashkin *et al.*, 1987, *Nature*, **330**, 769).

Laser cooling of atoms

Laser cooling of atoms can be observed when atoms in the beam are slowed by the light force from resonant scattering of oppositely-travelling laser beam. Consider a laser beam interacting with an atom resonantly so that when a photon is absorbed by the atom, its momentum is increased by h/λ (which is the momentum of photon) in the direction of the laser. When the atom re-emits the photon then its momentum is decreased, but there is no preferred direction for photon emission, i.e. the photon is said to be emitted a random selection. The same atom can reabsorb another photon from the laser and can re-emit again randomly so that on the average, the atoms moving in the direction of the laser beam are slowed down. However, the Doppler effect comes in the way of the moving atoms. An atom moving towards the laser beam finds the laser photon to be of slightly higher energy, and if the direction of the moving atom is opposite to that of the laser beam, then it will find the laser photon to be of lower energy. So, if an atom is placed between two laser beams (which are facing each other) with frequency slightly lower than the atomic resonance frequency then the laser on the left side of atom will slow down the moving atom towards left, as the Doppler shift of laser frequency will make the laser–atom interaction resonant. The laser on the left side of the atom and the atom moving in the right-hand direction will have very little interaction as the laser will be further detuned from the atomic transition. There will be exactly the opposite scenario with the laser on the right side, as this laser will cool down those atoms which are moving towards the right-hand side. In this way atom cooling in a single direction is obtained. If six lasers are employed in mutually perpendicular directions, then it is possible to have three-dimensional laser cooling of the atoms. Laser cooling can make the atoms reach temperature equivalent to single photon recoil energy ($< 1\ \mu K$).

Optical molasses

Three orthogonal pairs of laser beams (derived from the same laser having frequency slightly below atomic resonance frequency) along the cartesian axes forming standing waves slow the atom down, whichever direction it moves in. Hence in the intersection zone of laser beams, there is frictional or damping force exerted by the light, which is quite similar to particles moving in a viscous fluid. This arrangement is called an optical molass. The name was coined by Chu *et al.* (*Phys. Rev. Lett.*, 1985, **55**, 48) who first demonstrated this effect.

Quantum jumps

In the 19th century it had been well-established that atomic vapours emitted and absorbed light at discrete resonance wavelengths, a characterizing feature for a chemical element. At the beginning of the 20th century the quantum theory of atoms was developed by Bohr and others. They showed that these characteristic resonances or spectra were due to the quantum nature of atoms. According to Bohr, atoms are composed of discretized states of definite energy. Whenever transition occurs between allowed states, either emission or absorption of photons occurs. The change in atomic energy is related to frequency ν of the photon as $\Delta E = h\nu$, where h is the Planck's constant = 6.625×10^{-27} erg s. These instantaneous transitions were called 'quantum jumps'.

the ground state by electric quadrupole E_2 radiation or to the metastable $^2D_{5/2}$ level by magnetic dipole M_1 and E_2 radiation (in fact, E_2 decay rate to the $^2D_{5/2}$ level is negligible compared to M_1 rate). The $^2D_{5/2}$ level decays to the ground state by E_2 radiation. The magnetic quadrupole M_2 and electric octupole E_3 allowed decay rate from the $^2P_{1/2}$ level to the $^2D_{5/2}$ level is, however, much too small for experimental observation.

In the first set of experiments[16] with Hg^+ ion, the ion was simultaneously irradiated with two cw lasers driving the strong transition near 194 nm and the weak transition near 282 nm (see Figure 10 dashed line). The fluorescence signal from the laser-excited $^2S_{1/2} \rightarrow {}^2P_{1/2}$ resonance line was monitored. The abrupt cessation of fluorescence indicated a quantum jump to the metastable state $^2D_{3/2}$. When the ion jumped back from the metastable D state to the ground S state, the $S \rightarrow P$ resonance fluorescence signal returned instantaneously. Recent experiments on Hg^+ ion use only a single laser to excite the 194 nm strong transition. The four-level structure shown in Figure 10, allows one to predict quantum jumps. Experiments have observed these jumps and the data on the fluorescence signal have been used to determine the various radiative decay rates and also to infer the existence of photon antibunching.

We might also add here that Sauter *et al.*[15] have reported the observation of multiple quantum jumps, e.g. simultaneous quantum jumps of two or more ions when several Ba^+ ions were stored in the same trap. When two ions were in the trap, for example, the traces of the fluorescence signal showed three levels corresponding to both ions in the 'on' state, and one ion in the 'on' state and the other in the 'off' state. They attributed this phenomenon to a cooperative interaction between the atoms and the radiation field. Recent experiments[17] on Hg^+ ions have, however, shown that simultaneous or cooperative jumps are rare. The three levels of fluorescence observed when two Hg^+ ions were trapped were interpreted as due to independent ion jumps, rather than collective jumps.

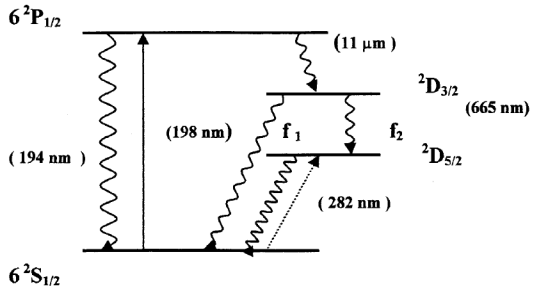

Figure 10. Level structure of Hg^+ ion used in quantum jump experiments. In the first series of experiments, the ion was irradiated with two cw lasers simultaneously driving the strong transition $^2S_{1/2} \rightarrow {}^2P_{1/2}$ and the weak transition $^2S_{1/2} \rightarrow {}^2D_{5/2}$. In a later experiment, only one laser driving the strong transition was used.

Quantum jumps have also been observed in single Mg^+ ions in a Penning trap[18]. The level structure of Mg^+ ion is shown in Figure 11. A single 280 nm laser was tuned close to the $m_J = -1/2$ to $m_J = -3/2$ Zeeman component of the transition from the $3s^2S_{1/2}$ ground level to the $3p^2P_{3/2}$ level. The laser was linearly polarized with the polarization direction perpendicular to the direction of the magnetic field, so that only $\Delta m_J = \pm 1$ transition was allowed. The laser detuning is denoted by Δ, the radiative decay constant of each excited level is γ and the energy separation is $\alpha/2$ (ref. 18). The dipole decay is allowed from level 3 to level 1 only, so that the fluorescence will be observed continuously until level 5 is populated from level 1 due to non-resonant transition (indicated by dashed arrow in the Figure 11) caused by the finite linewidth of this transition overlapping with the laser. Once level 5 is populated, then this level can decay back to level 1 with probability 1/3 (indicated as wavy arrow $\gamma/3$ in Figure 11) and thus the $1 \leftrightarrow 3$ transition continues. On the other hand, if level 5 decays to level 2 by a spontaneous Raman transition (with probability 2/3, indicated as wavy arrow $2\gamma/3$ in Figure 11), then it remains there and fluorescence will be terminated. However, due to off-resonant excitation, an atom can move from level 2 to level 4 (dipole allowed) and then decay back to level 1 (the entire process is an off-resonant Raman transition[18]) to restart the fluorescence. The experimental trace of the fluorescence showed that the mean ratio was found to be nearly independent of the intensity of the laser because of the existence of coherence between excited levels. The experimental results also verified an effective two-state rate equation description of the dynamics of the quantum jumps.

So far we have not discussed the utility of quantum jump experiments in realization of any potential quantum information processor! The ion traps have been suggested as one of the possible and most potent quantum informa-

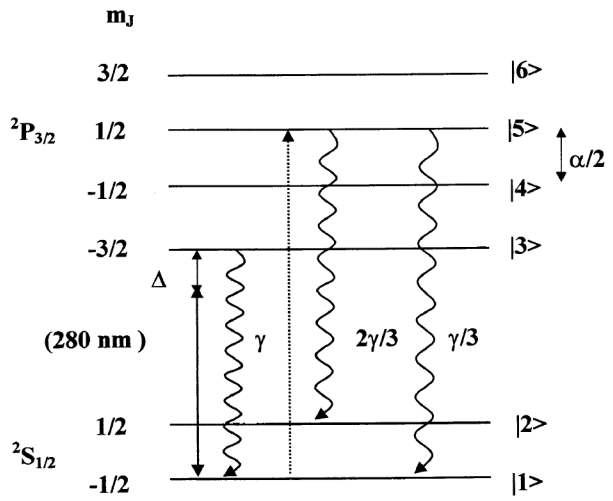

Figure 11. Energy level diagram for the $^2S_{1/2}$ and $^2P_{1/2}$ lines of Mg^+ ion in a magnetic field. A laser of frequency ω is used to drive the transition $|1\rangle \rightarrow |3\rangle$. Laser polarization allows only $\Delta m = \pm 1$ transition.

tion processors where the required entanglement can be generated with the present technology. Many proposals and pioneering experiments have come up after the proposal of Cirac and Zoller[19] for an ion trap quantum computer. Hughes *et al.*[20] have proposed that the ion traps could provide a possibility of realizing a practical quantum computer of long-term success.

Though most of the physics of ion traps is well understood, some experiments have displayed unexplained collective behaviour in the presence of several identical ions. The collective behaviour has been manifested as an enhanced rate of coincident quantum jumps. In the experiment of Sauter *et al.*[15] (as discussed above) on a system of three trapped ions of Ba^+, it was observed that the measured two-fold and three-fold coincident quantum jumps increased by two orders of magnitude compared to what is expected on the basis of statistics. A possibility of collective interaction of ions with the electromagnetic field has been proposed[21]. However, in the experiments by Itano *et al.*[17] on two and three Hg^+ ions, no such correlations were observed. More precisely, in a test of two ions they observed 5649 quantum jumps consecutively, in which the number of double jumps was about 11, which was within the experimental error of random coincidences. Later, Werth's group[22] also reported enhancement of two-fold and three-fold coincidence rates in a linear chain of Ca^+ ions containing 10 identical species. Perhaps there is a long-range interaction in the linear ion crystal. So, what is the fallout of the experiments by Sauter *et al.*[15] and Block *et al.*[22]? Since only electromagnetic interaction is involved, any new physical effect or interaction is unlikely on the basis of these observations. But if their observations are correct, then there is serious doubt about the suitability of ion traps as a quantum information processing device.

The physics of interaction responsible for these collective effects should be well understood in order to take care of the quantum error correction (QEC). In order to understand this problem in a systematic manner, Stacey's group[23] has taken up some experiments. One such experiment involves a linear chain of 2 or 3 trapped Ca^+ ions. Their work is complimentary to that of Itano *et al.*[17] and they have used different time scales. They have observed double quantum jumps of about 0.05% of the single quantum jump rate, which is quite similar to the work of Itano *et al.* The methodology adopted in the work of Stacey's group is similar to that in the experiment of Block *et al.*[22]. In their experiment[23] on $^{40}Ca^+$ ions, a linear Paul trap in vacuum ($< 2 \times 10^{-11}$ Torr) has been used with ion separation of 15 μm. The laser cooling technique is used for obtaining temperature of a few mK for these ions. The energy level diagram of $^{40}Ca^+$ is shown in the Figure 12. The ions are continuously illuminated with lasers tuned at the transitions 397 nm and 866 nm and the fluorescence at 397 nm is detected by a photomultiplier detection system. Another laser at 850 nm drives the $3D_{3/2} \rightarrow 4P_{3/2}$ transition. The most likely route for the decay of $4P_{3/2}$ is to $4S_{1/2}$ ground state, but it can go back to $3D_{3/2}$. About 1 in 18 decays proceed to $3D_{5/2}$ metastable or the shelving level. If the ion is shelved, then the fluorescence is stopped. All ions get shelved within 100 ms – the duration for which 850 nm laser beam remains open. By use of specialized techniques described in ref. 23, they have observed quantum jumps from the metastable $3d^2D_{5/2}$ levels were observed for several hours in order to search for correlations between decay time of the different ions. No correlation was observed, thus keeping our hopes alive for an ion trap quantum processor.

Theoretical formulation and interpretation of quantum jumps

Basic equations for atomic evolution

We outline a theory for testing the interaction of a two-level atom with a coherent field. The Hamiltonian of such a system has the form

$$H = H_a + H_R + H_{a-R} + H_{a-C}, \tag{21}$$

where the various terms are

$$H_a = \hbar\omega_0 S_+ S_-, \quad H_R = \hbar\Sigma\omega_k b_k^\dagger b_k, \tag{22}$$

$$H_{a-R} = -\hbar(\overline{\lambda E_2})S_+ - \hbar(\overline{\lambda}^* \overline{E}_2^\dagger)S_-, \tag{23}$$

$$H_{a-C} = -\hbar(\overline{\lambda E_C})S_+ - \hbar(\overline{\lambda}^* \overline{E}_C^\dagger)S_-. \tag{24}$$

Here $S_\pm$ are the atomic raising and lowering operators

$$S_+ = |2\rangle\langle 1|, \quad S_- = |1\rangle\langle 2|. \tag{25}$$

The radiation field modes are characterized by b_k, $b_k^\dagger$ and

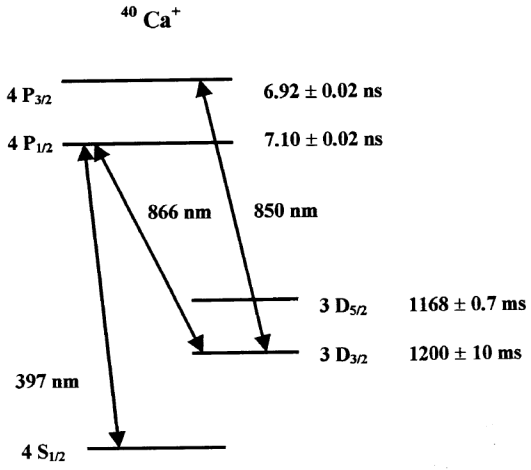

Figure 12. Schematic of $^{40}Ca^+$ energy-levels along with their lifetimes and the wavelengths of lasers (in nm) driving them.

$$\bar{E}_R = i\sum_k \left(\frac{\hbar\omega_k}{2\varepsilon_0 V}\right)^{1/2} b_k \hat{e}_k , \tag{26}$$

where $\hat{e}_k$ is the polarization vector and $\bar{E}_C(t)$ is the applied coherent field. Finally, the dipole matrix element is given by

$$\hbar\bar{\lambda} = \langle 1 | \bar{d} | 2 \rangle . \tag{27}$$

Dipole approximation and rotating wave approximation are implicit in the Hamiltonian. The dynamics may be described by the total density operator ρ_T, ($T = a + R$) obeying the Liouville–von Neumann equation

$$i\hbar \frac{\partial \rho_T}{\partial t} = [H, \rho_T]. \tag{28}$$

This equation contains all the dynamics, but is too general to be of use in practice. In order to extract useful information from it, we may consider two levels of description.

Reduced atomic density operator ρ: We concentrate only on the atomic evolution and ignore the details of reservoir photons. Here we have a reduced description in terms of the atomic density operator $\rho = Tr_R \rho_T$. The equation for ρ is obtained by standard techniques. A rather transparent derivation is obtained by Mollow[24]. The basic result of a system (atom) interacting with an infinite reservoir (bath of photons) is to introduce damping (atomic decay) and an energy shift (incorporated by renormalizing the atomic transition frequency ω_0). The resulting equation reads as

$$\frac{d\rho}{dt} = -\frac{i}{h}(H_{\text{eff}}\rho - \rho H_{\text{eff}}^{\dagger}) + 2\gamma S_- \rho S_+ . \tag{29}$$

Here H_{eff} is an effective Hamiltonian.

$$H_{\text{eff}} = \hbar(\omega_0 - i\gamma)S_+S_- - \hbar(\bar{\lambda}^* \cdot \bar{E}_C^* S_- + \bar{\lambda}\bar{E}_C S_+). \tag{30}$$

Optical Bloch equations are obtained by taking the matrix elements between the atomic states and defining $\rho_{ij} = \langle i|\rho|j\rangle$.

Atomic density operator in the subspace of n photons: Here we are interested in the subspace of the total Hilbert space, where the atom is in any of the two states but the radiation field contains exactly 'n' photons. The reduced density operator $\rho^{(n)}$ in the subspace containing n fluorescent photons evolves according to the equation

$$\frac{d\rho^{(n)}}{dt} = -\frac{i}{\hbar}(H_{\text{eff}}\rho^{(n)} - \rho^{(n)}H_{\text{eff}}^{\dagger}) + 2\gamma S_- \rho^{(n-1)} S_+ (1-\delta_{n0}). \tag{31}$$

This equation is inhomogeneous due to the presence of a source term representing the atomic transition $|1\rangle \rightarrow |2\rangle$ accompanied by the emission of the nth photon. The reduced atomic density is simply given by

$$\rho(t) = \sum_{n=0}^{\infty} \rho^{(n)}(t). \tag{32}$$

In the particular case of $n = 0$ (no fluorescence photon), we have

$$\frac{d\rho^{(0)}}{dt} = -\frac{i}{\hbar}(H_{\text{eff}}\rho^{(0)} - \rho^{(0)}H_{\text{eff}}^{\dagger}). \tag{33}$$

This equation describes the coherent evolution of the atom without emission of a photon.

Delay function, survival probability and $g^{(2)}(t)$

The second level of description is particularly useful for interpreting many quantum-optics phenomena, such as resonance fluorescence spectra, photon statistics and quantum jumps. The important quantity is the probability distribution of the time interval between the emission of two successive photons $w(t)$. This is called the delay function or waiting time distribution.

The survival probability $P(t)$ is defined as the probability that no photon emission has occurred by the delay time t. Clearly,

$$P(t) = 1 - \int_0^t w(t')\, dt', \tag{34}$$

$$w(t) = -\frac{dP}{dt}. \tag{35}$$

In order to obtain the relation between $g^{(2)}(t)$ and $w(t)$, we introduce another correlation function $Q(t)$. $Q(t)\,dt$ is the conditional probability that the atom radiates any photon between t and $t + dt$ after it has emitted one at $t = 0$. The photon emitted at t can be the first photon after the one at $t = 0$, or the next after any one at $t'(0 < t' < t)$. Thus

$$Q(t) = w(t) + \int_0^t dt' Q(t') w(t - t'). \tag{36}$$

Alternatively, the photon at t is either the first photon following the one at $t = 0$ or any one after the next at t' $(0 < t' < t)$. Hence

$$Q(t) = w(t) + \int_0^t dt' Q(t' - t') w(t'). \tag{37}$$

The second-order intensity correlation is then given by

$$g^{(2)}(t) = Q(t)/Q(\infty). \tag{38}$$

Wave function approach

It has been suggested that the atomic operator master equation describing a photo-emission process is equivalent to a stochastic quantum mapping. Quantum evolution

of such a system under a non-unitary Schrödinger equation corresponds to an iteration of the quantum mapping obtained for a random time interval and at the end of this interval there is wavefunction collapse[25]. The quantum evolution is a sensitive function of the past history of the photoemissive process and the calculation of probabilities depends on the past history. In general, the analytical method to implement this quantum mapping is difficult, but numerical simulation generates 'quantum trajectories' for stochastic wave function. Such a trajectory is good enough to quantify the current status of the quantum-mechanical system with a past history of evolution and wave-function collapse. A time series can be obtained from these trajectories which is statistically equivalent to fluctuating signals obtained from a single quantum system. These trajectories can be used to analyse quantum jumps, photon scattering in cavity QED and degenerate parametric oscillators[25]. In the following we will discuss briefly the wavefunction approach for the resonance fluorescence.

The form of the evolution eq. (31) suggests that it is possible to revert to wave-function approach using Schrödinger equation with the non-Hermitian Hamiltonian H_{eff}:

$$i\hbar \frac{\mathrm{d}|\psi(t)\rangle}{\mathrm{d}t} = H_{\text{eff}}|\psi(t)\rangle, \tag{39}$$

$$|\psi(t)\rangle = C_1(t)\ |1, n\rangle + C_2(t)\ |2, n\rangle. \tag{40}$$

As a procedure to compute the survival probability $P(t)$ and therefrom the delay function $w(t)$ and $g^{(2)}(t)$, this approach is just all right. However, the free non-unitary evolution is interrupted by quantum jumps and when delay function $w(t)$ is analytically available, one can introduce an efficient random sampling technique or Monte-Carlo procedure for the analysis of the process. After the emission of the nth photon at time t_n, the atom is in its ground state and the choice of the single random number determines the time t_{n+1} of the emission of the $(n + 1)$th photon. This type of Monte-Carlo approach is of much current interest[25] and has advantage in more complex situations, where solving the density matrix equation becomes difficult and time-consuming.

We assume that the two-level atom is evolving in a coherent superposition of its two states $|1\rangle$ and $|2\rangle$ for a time t, without emitting a photon. The Schrödinger equation is

$$i\hbar \frac{|\psi(t)\rangle}{\mathrm{d}t} = (\hbar(\omega_0 - i\gamma)S_+S_-$$

$$-\hbar\Omega(\mathrm{e}^{-\omega_L t}S_+ + \mathrm{e}^{+\omega_L t}S_-))|\psi(t)\rangle, \tag{41}$$

where $\Omega = (\mathrm{d}\cdot E_c)/2\hbar$ is one half of the Rabi frequency, and

$$|\psi(t)\rangle = C_1(t)|1, 0\rangle + C_2(t)|2, 0\rangle, \tag{42}$$

there being no photons in the field and $|i, 0\rangle = |i\rangle_a|0\rangle_R$.

It is easy to show that $C_i(t)$ satisfies the following equations

$$\dot{C}_1 = -(i\omega_0 + \gamma)C_1 - i\Omega C_2\mathrm{e}^{-i\omega_L t}, \tag{43}$$

$$\dot{C}_2 = -i\Omega C_1\mathrm{e}^{i\omega_L t}. \tag{44}$$

These equations can be solved easily. At exact resonance, assuming the atom to be in the ground state initially ($C_2 = 1$), we obtain

$$C_1(t) = \frac{i\Omega}{\lambda}\mathrm{e}^{-(i\omega_L - \gamma/2)t}\sinh(\lambda t), \tag{45}$$

$$C_2(t) = \left(\frac{\gamma}{2\lambda}\sinh(\lambda t) + \cosh(\lambda t)\right)\mathrm{e}^{-\gamma t/2}, \tag{46}$$

where $\lambda = (\gamma^2 - 4\Omega^2)^{1/2}/2$. The survival probability $P(t)$ and the delay function $w(t)$ are given by

$$P(t) = |C_1|^2 + |C_2|^2$$

$$= \mathrm{e}^{-\gamma t}\left[\frac{\gamma}{2\lambda}\sinh(2\lambda t) + \frac{\gamma^2}{4\lambda^2}\cosh(2\lambda t) - \frac{\Omega^2}{\lambda^2}\right], \tag{47}$$

and

$$w(t) = -\gamma(\Omega/\lambda)^2\,\mathrm{e}^{-\gamma t}[1 - \cos(2\lambda t)]. \tag{48}$$

Note here that $w(0) = 0$ implies antibunching, i.e. the photons tend to repel each other. The expression for $Q(t)$ and $g^{(2)}(t)$ may be obtained from $w(t)$. In particular,

$$g^{(2)}(t) = \mathrm{e}^{-\gamma t}\left[1 - \left(\frac{3\gamma}{2\mu}\sinh(\mu t) + \cosh(\mu t)\right)\mathrm{e}^{-3\gamma t/2}\right], \tag{49}$$

where $\mu = (\gamma^2 - 16\Omega^2)^{1/2}/2$. Clearly $g^{(2)}(0) = 0$ and in the limiting cases of weak and intense fields, the above expression simplifies to eq. (9).

Theories of quantum jumps

Cook and Kimble's analysis on quantum jumps inspired many theoretical papers on the interpretation of such jumps. The basic question is: what leads to the random telegraph? While Cook and Kimble's analysis refers to incoherent excitation, experimental realization of the Dehmelt scheme requires one or more coherent fields. The ion is thus in a coherent superposition of the three states (Figure 7 *a*) instead of in individual atomic states.

Naturally, one needs a theory involving the density matrix ρ. The diagonal elements $\rho_{ii} = \langle i|\rho|i\rangle$ represent the probabilities of an ion being in state $|i\rangle$, while the off-diagonal elements $\rho_{ij} = \langle i|\rho|j\rangle$, $(i \neq j)$ imply, crudely speaking, that the ion is simultaneously occupying all levels. The nine components of the density matrix satisfy the so-called Bloch equations. Note that for incoherent excitation, fluctuations in the light field destroy quantum-mechanical coherence; this results in rate equations which can be interpreted in terms of a (classical) probability of finding the ion in one of the atomic states rather than in a superposition of these states.

We briefly review some of the theoretical papers here. Javanainen[26] has treated the scheme of Figure 7 *b* with a strong transition $|3\rangle \leftrightarrow |1\rangle$ excited by a coherent field coupled weakly to a metastable third level $|2\rangle$. He calculated multi-time distribution function for photon emissions from the strong transition. For a single trapped ion, this multi-time distribution can be factorized into products of two-time distributions. In the stationary limit, the basic quantity of interest is thus the normalized intensity–intensity correlation function $g^{(2)}(t)$ which is a measure of the probability for photon emission at a time t, after an earlier emission at time zero. In the limit of an infinite Rabi frequency for strong transition, Javanainen's analysis[26] results in rate equations analogous to those of Cook and Kimble. The long time behaviour of the correlation $g^{(2)}(t)$ is then related to a dichromatic Markov process. Schenzle *et al.*[27] consider a three-level atom with fully saturating and incoherent excitation. From both the short and long time behaviour of the intensity correlation function $g^{(2)}(t)$, they could conclude the existence of quantum jumps of the atom which are reflected as intermittent dark and bright periods of fluorescence.

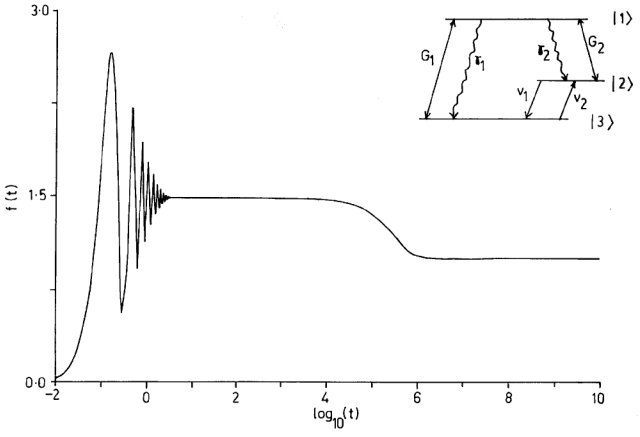

Figure 13. Normalized intensity–intensity correlation function $f(t)$ as a function of time for $\gamma_1 = 1$, $\gamma_2 = 10^{-6}$, $\nu_1 = 10^{-6}$, $\nu_2 = 0$, $G_2 = 0$. Here G_i $(i = 1, 2)$ are Rabi frequencies of two fields, γ_i $(i = 1, 2)$ are radiative decay constants and ν_i $(i = 1, 2)$ are non-radiative transition rates. For short times it exhibits the familiar antibunching and Rabi oscillations. Transition between two different steady states, one on the time scale $\gamma_1 t \geq 1$ and the other $\gamma_2 t \geq 1$, occurs for $\gamma_1 t \gg 1$, $\gamma_2 t \leq 1$. For further details see ref. 35.

In a subsequent paper, Schenzle and Brewer[28] discuss photon-counting statistics of the dark periods from higher order correlation functions. The same configuration is also treated by Kimble *et al.*[29], who have evaluated the intensity correlation function for resonant monochromatic excitation of the strong transition.

A somewhat different interpretation of the quantum jumps was given by Cohen-Tannoudji and Dalibard[30] who consider the case of monochromatic excitation of both transitions (Figure 7 *a*). They point out that with the excitation on a weak line, the strong resonance fluorescence develops an extra probability for the next photon to appear after a long time interval. The relevant quantity to study is, therefore, not the intensity correlation function $g^{(2)}(t)$, but the waiting time distribution $w(t)$. The latter is defined as the distribution of the time intervals t that one has to wait after the emission of a photon before the next one is emitted. The presence of weak, but slowly decaying long-time tail in the distribution is a manifestation of the existence of long dark periods in the fluorescence. Similar waiting-time distribution has also been studied by Zoller *et al.*[31] assuming incoherent excitation with complete saturation. The waiting-time distribution $w(t)$ is however, related in a simple way to the intensity correlation function. This has been pointed out by Kim *et al.*[32] and Nienhuis[33].

We might also add that Pegg *et al.*[34] and Kimble *et al.*[29] have pointed out that a key role in the occurrence of quantum jumps in the coherently excited three-level atom is taken by the dressed-atom Autler–Townes splitting which governs the intensity-dependent resonance condition. Quantum jumps in a coherently-driven Raman system (Figure 7 *b*) were studied by Agarwal *et al.* and by others[35]. Physical quantities of interest are the intensities and the intensity–intensity correlations $f(\tau)$ and $g(\tau)$ in the stationary limit. The behaviour of $f(\tau)$ and $g(\tau)$ is shown in Figures 13–15. It is seen that the correlations show damped Rabi oscillations in the region $t \leq \gamma_1^{-1}$, a transition region $\gamma_1^{-1} \ll t \leq \gamma_2^{-1}$ and finally a steady state.

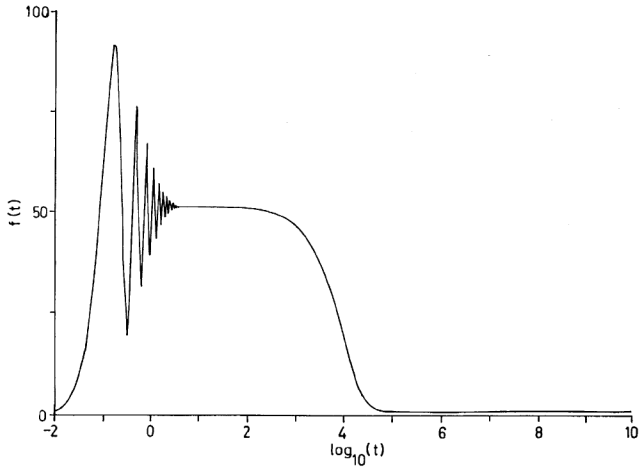

Figure 14. Same as Figure 13, but for $G_2 = 0.1$.

Box 2.

Bose–Einstein condensation

The Bose–Einstein condensation (BEC) observed by Cornell, Weimann, Ketterle and Hulet in 1995, was predicted about 70 years ago. In this particular state of matter, the individual atoms lose their identity and all the atoms condense into the same quantum state and act as a single entity, but its behaviour is quantum mechanical in nature on a macroscopic scale. The BEC state which is a phase transition, is very important for superfluidity, superconductivity and spontaneous symmetry-breaking in field theory. When indistinguishable boson (having integral spin) are cooled down to such a low temperature that the separation between atoms is of the order of their de-Broglie wavelength, the phenomenon of BEC takes place. To observe this phenomenon, researchers have used combination of laser cooling along with evaporative cooling. Collisions with very low energy scattering amplitudes are the characterizing features of a BEC. At very low temperature, the 's-wave' collision is predominant where its amplitude becomes independent of energy. The scattering length could be positive or negative depending on the inter-atomic potential. A BEC will be stable if the scattering length of low energy collision is positive.

Atom laser vs optical laser

A laser is an amplifier of optical light waves. The corresponding matter-wave amplifier can be called the atom laser. An optical amplifier or the laser consists of a gain medium which contains either atoms or molecules each having at least three energy levels or more. In a three-level laser, atoms are pumped from the ground (or lower) state $|g\rangle$ to the excited (upper) state $|e\rangle$ by means of some pumping mechanism, viz. a flash lamp, a plasma or another laser. The presence of an optical input wave whose frequency matches with the transition $|e\rangle$ to $|l\rangle$ stimulates the atom to move to the state $|l\rangle$ by emitting optical radiation in the same direction with the same phase and at the same wavelength as the input optical wave. The entire process is called stimulated emission or more precisely light amplification by stimulated emission of radiation (LASER). 'Coherence' is an important property of lasers. ['Coherence' means a fixed phase relationship between light waves in a beam of light. Two wavetrains of light are coherent when they are in phase, i.e. vibrate in unison, and are incoherent if there is random phase relationship. 'Coherence' for laser is used to describe relations between phases within the same beam.] The 'atom-laser' was thought of to be similar to the optical laser and initial developments were based on coherent extraction of atomic beam from a Bose–Einstein condensate. But do we really amplify atoms? This question went unanswered. In yet another development, the phase-coherent matter-wave amplification by stimulated emission of atoms has been demonstrated and it is considered to be quite close to a true atom laser. In principle, the matter-wave amplifier is analogous to the optical amplifier or laser in the sense that in former, the stimulated emission of atoms takes place rather than those of the photons. One important difference between the two systems is that photons can be created out of vacuum but not atoms. So atoms in the matter-wave amplifier cannot be created like photons in optical lasers. However, the creation of atoms in the matter-wave amplifier can be engineered by allowing the gain medium to serve as a reservoir of atoms. The gain medium considered here is a Bose–Einstein condensate and the energy level diagram is as shown in the accompanying figure (***b***).

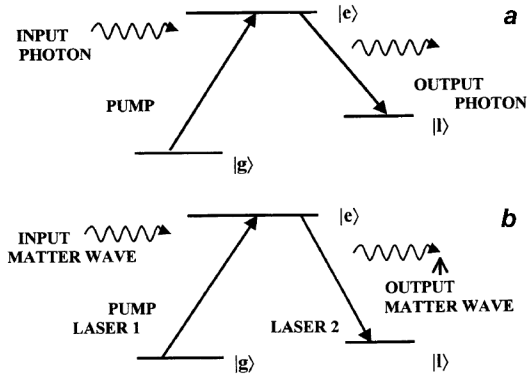

The pumping from the level $|g\rangle$ to $|e\rangle$ is done by a laser 1 in this case and the input matter-wave is prepared using optically induced Bragg's diffraction of a Bose–Einstein condensate (BEC) gain medium. The atom of BEC in the state $|e\rangle$ can emit a photon of different frequency (other than that from the pump) and may go to level $|l\rangle$ by spontaneous emission having random phase. If the atom interacts with the matter-wave (generated by Bragg diffraction using laser 2) before the spontaneous emission then the excited atom in state $|e\rangle$ is more likely to go to state $|l\rangle$ with the same velocity and phase as the input wave and a phase coherence is built-up. As a result, an intense matter-wave emerges and all the excited atoms of the gain medium are shifted to state $|l\rangle$. In a recent experiment, Inouye *et al.* (*Nature*, 1999, **402**, 641) observed a gain of 10 to 100 in their matter-wave amplifier. Their amplifier has produced more intense stimulated wave but otherwise identical to the input wave, thus maintaining phase coherence. The phase coherence was verified with the help of interferometry.

It is also important to note that the rate of decay in the transition region can be controlled by the strength of the field driving the transition $|1\rangle \rightarrow |2\rangle$ (see Figure 13). It is clear from Figure 14 that the intensity correlation $g(t)$ gives an indication of the upward jump from an 'off' state to an 'on' state. Physically, the system is in the 'off' state after the Stokes photon is detected. Thus, if at some time later a Rayleigh photon has been detected, it obviously implies a jump to the 'on' state. Also, the probability of detecting two Stokes photons will be much smaller due to overall scale factor $\alpha_2^2/(\alpha_1^2 + \alpha_2^2)$. In the Λ system (a Λ system means the configuration of three levels has been made in such a way that it looks like the Greek symbol capital lambda), the quantum jump appears to be from the strongly fluorescent manifold of dressed states $|\psi_1\rangle$ and $|\psi_3\rangle$ and the non-radiative dressed states $|\psi_2\rangle$. In the particular case of $\alpha_2 = 0$, the shelving theory is clearly applicable.

Quantum jumps in a V-system

The interpretation of observed quantum jumps in a V-system (a V-system means the configuration of three levels which looks like the Roman alphabet capital 'vee') is rather interesting. Here the simple shelving theory based on Schrödinger cat dichotomy seems to be inapplicable. Quantum mechanically, at any instant of time, the atom is in a superposition of all three states. According to quantum measurement theory, when a photon is detected, this superposed state collapses to the single ground state. Then how can we explain the existence of periods of prolonged darkness? The answer lies in the expression for survival probability $P(t)$ or for the delay function $w(t)$. As before, we consider the coherent evolution of the ion described by the Schrödinger equation

$$i\frac{\partial|\psi(t)\rangle}{\partial t} = H_{\text{eff}}|\psi(t)\rangle \tag{50}$$

where

$$|\psi\rangle = \sum_{i=1}^{3} C_i(t)|i,\ (0)\rangle, \tag{51}$$

$$H_{\text{eff}} = \hbar(\omega_{13} - i\gamma_1)A_{11} + \hbar(\omega_{23} - i\gamma_2)A_{22} + \hbar\alpha_1(e^{-i\omega_{L1}t}A_{13} + hc) + \hbar\alpha_2(e^{-i\omega_{L2}t}A_{23} + hc), \tag{52}$$

and $2\alpha_i$ (i = 1, 2) are the Rabi frequencies.

The coefficients $C_i(t)$ are determined from the equations

$$\dot{C}_1 = -i(\omega_{13} - i\gamma_1)C_1 - i\alpha_1 e^{-i\omega_{L1}t}C_3, \tag{53}$$

$$\dot{C}_2 = -i(\omega_{23} - i\gamma_2)C_2 - i\alpha_2 e^{-i\omega_{L2}t}C_3, \tag{54}$$

$$\dot{C}_3 = -i\alpha_1 e^{+i\omega_{L1}t}C_1 - i\alpha_2 e^{+i\omega_{L2}t}C_2. \tag{55}$$

The rapidly oscillating factors may be removed by making a transformation

$$C_1 = b_1 e^{-i\omega_{L1}t},\ C_2 = b_2 e^{-i\omega_{L2}t},\ C_3 = b_3, \tag{56}$$

and the resulting equations for $b_i(t)$ read as

$$\dot{b}_1 = (i\Delta_1 - \gamma_1)b_1 - i\alpha_1 b_3, \tag{57}$$

$$\dot{b}_2 = (i\Delta_2 - \gamma_2)b_2 - i\alpha_2 b_3, \tag{58}$$

$$\dot{b}_3 = -i\alpha_1 b_1 - i\alpha_2 b_2, \tag{59}$$

where $\Delta_1 = \omega_{L1} - \omega_{13}$, $\Delta_2 = \omega_{L2} - \omega_{23}$. Equations (57–59) can be solved under the initial conditions $b_1(0) = b_2(0) = 0$ and $b_3(0) = 1$ (ion initially in the ground state $|3\rangle$). We use the quantum jump conditions $\gamma_1 \gg \gamma_2$, $\alpha_2 \ll \alpha_1$, $\alpha_2 \ll \gamma_1$ and set $\Delta_1 = 0$. The survival probability $P(t)$ is then given by

$$P(t) = |b_1|^2 + |b_2|^2 + |b_3|^2 = \frac{1}{\lambda^2}[4\alpha_1^2 - \gamma_1^2\cos(\lambda t) + \gamma_1\lambda\sin(\lambda t)]\,e^{-\gamma_1 t} + |\alpha|^2 e^{-2\Gamma t}, \tag{60}$$

where

$$|\alpha|^2 = \left|\frac{i\varepsilon}{\alpha_2}\right| = \frac{\alpha_2^2(\gamma_1^2 + \Delta_2^2)}{(\alpha_1^2 - \Delta_2^2) + \gamma_1^2\Delta_2^2},$$

$$\lambda = (4\alpha^2 - \gamma^2)^{1/2},$$

$$\Gamma = \gamma_2 + \frac{\gamma_1\alpha_1\alpha_2^2}{(\alpha_1^2 - \Delta_2^2) + \gamma_1^2\Delta_2^2}. \tag{61}$$

The survival probability $P(t)$ is explicitly decomposed

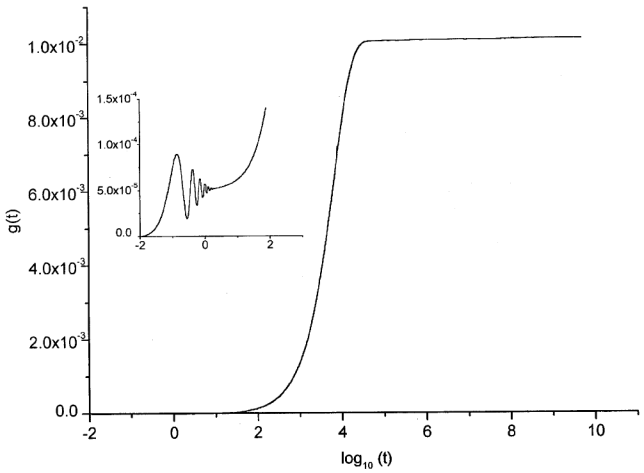

Figure 15. The cross correlation function $g(t) = \langle T_N[I_S(t')I_R(t'+t)]\rangle / [\langle I_S\rangle\langle I_R\rangle]$ as a function of time for $G_1 = 10$, $G_2 = 0.1$, $\gamma_2 = 10^{-6}$, $\nu_1 = 10^{-6}$. Note the jump to the 'on' state for $\gamma_1 t \leq 10^4$. (*Inset*) Oscillatory regime of $g(t)$ on an enlarged scale.

into two parts. The rapid decay follows the two-level atomic dynamics, whereas the slow decay function has the coefficient $|\alpha|^2$ and the decay rate 2Γ.

The probability that, after a reset, there will be a dark period of length greater than $t > 1/\gamma_1$ is given by

$$P_2(t) = (|b_{12}|^2 + |b_{22}|^2 + |b_{32}|^2) \exp[(\lambda_2 + \lambda_2^*)t] \approx |\alpha|^2 e^{-2\Gamma t}. \quad (62)$$

For a resonantly-tuned coupling to level $|2\rangle$ so that $\Delta_2 = \alpha_1$, the long time (dark) probability to be in the level $|1\rangle$ is lower from that to be in the metastable level $|2\rangle$ by the factor

$$\frac{|b_{12}|^2}{|b_{22}|^2} = \alpha_2^2/\gamma_1^2. \quad (63)$$

Thus regardless of the length of the period, there is still a finite probability that the atom is shelved in the allowed level $|1\rangle$ as opposed to the forbidden level $|2\rangle$. The probability that a dark period will end with the emission of a strong transition $|1\rangle \rightarrow |3\rangle$ photon compared to ending with a $|2\rangle \rightarrow |3\rangle$ photon is

$$\frac{\gamma_1 |b_{12}|^2}{\gamma_2 |b_{22}|^2} = \alpha_2^2/(\gamma_1\gamma_2), \quad (64)$$

which need not be small. If it is large, there is a large probability that a dark period ends with the emission of $|1\rangle \rightarrow |3\rangle$ photon. In other words, the inherent quantum indeterminacy is reflected in the fact that a dark period can end with the emission of a photon of any colour (Figure 16)!

Quantum Zeno effect

Quantum mechanical prediction of an event involves two aspects. The first is the dynamics – the unitary evolution (U) in time of the state of the system. The state carries the information about all observable possibilities. The second aspect is the reduction R of the state vector. The reduction needs a measurement of some property of the system. The latter operation singles out one of the possible outcomes. It turns out however, that the act of the measurement intervenes. The quantum Zeno effect has to do with the interplay between observation and intervention in quantum systems[36] that a continuously observed state can never decay. A 'watched pot' never boils! Achilles, who is cynosure of all eyes, fails to win!

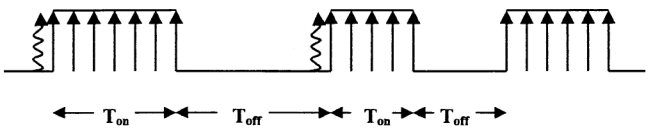

Figure 16. Time structure of fluorescence telegraph in V-system. Dark periods may end with the emission of either a strong photon or a weak photon.

Consider a quantum system initially in an unstable state. We may introduce the notion of survival probability $P(t)$ of finding the system in the initial state after being left to itself for a certain period of time t. The Zeno effect implies that the survival probability $P(t)$ tends to unity in the limit of a continuous series of observations intended to find out whether the system is in the original state or not. This effect is a consequence of two factors: (a) presence of an initial range of time for which the survival probability falls off as t^2, and (b) notion of the reduction of the state vector or the wavefunction collapse during observation.

We may illustrate the first factor by the following heuristic considerations. Consider, Heisenberg's uncertainty relations for the observables characterized by non-commuting operators $\hat{A}$ and $\hat{B}$.

$$\Delta\hat{A}\,\Delta\hat{B} \geq \tfrac{1}{2}|\langle[\hat{A},\hat{B}]\rangle, \quad (65)$$

where

$$(\Delta\hat{A})^2 = \langle\hat{A}^2\rangle - \langle\hat{A}\rangle^2. \quad (66)$$

The operator $\hat{A}$ evolves according to Heisenberg's equation of motion and, in particular, we have

$$i\hbar\frac{\mathrm{d}}{\mathrm{d}t}\langle\hat{A}\rangle = \langle[\hat{A},\hat{H}]\rangle|. \quad (67)$$

If we assume $\hat{B} = \hat{H}$, then it is clear from eqs (65) and (67) that

$$\Delta\hat{A} \geq \frac{\hbar}{2(\Delta E)}\left|\frac{\mathrm{d}\langle\hat{A}\rangle}{\mathrm{d}t}\right|, \quad (68)$$

where ΔE is uncertainty in energy. Now let $\hat{A} = |\psi\rangle\langle\psi|$ be the projection operator with $|\psi\rangle$ as the initial decaying wavefunction and let $|\phi\rangle$ be the wavefunction at time t. Clearly,

$$|\phi(t)\rangle = \exp\left(-\frac{it\hat{H}}{\hbar}\right)|\psi\rangle. \quad (69)$$

Then it follows that

$$\langle\hat{A}(t)\rangle = \langle\hat{A}^2(t)\rangle = P(t) = |\langle\psi|\phi\rangle|^2, \quad (70)$$

$$(\Delta\hat{A})^2 = P(1-P), \quad (71)$$

and eq. (68) takes the form

$$[P(1-P)]^{1/2} \geq \frac{\hbar}{2\Delta E}\left|\frac{\mathrm{d}P}{\mathrm{d}t}\right|, \quad (72)$$

where $P = 1$ at $t = 0$ (initially). Since the RHS of eq. (72) is positive definite, it follows that

$$\frac{dP}{dt} = 0 \text{ at } t = 0, \tag{73}$$

provided that $\Delta E = \langle \hat{H}^2 \rangle - \langle \hat{H} \rangle^2$ is finite. This implies that there is no linear term in $P(t)$, i.e. the survival probability falls as t^2:

$$P(t) = 1 - at^2 + \ldots, \tag{74}$$

for small times. More precisely, if we write eq. (72) in the form

$$\frac{dP}{[P(1-P)]^{1/2}} \leq \frac{2}{\hbar}(\Delta E)\, dt, \tag{75}$$

and integrate both sides, we obtain the inequality known as Fleming's rule

$$P(t) \geq \cos^2((DE)t/\hbar), \tag{76}$$

which again reflects the behaviour predicted in eq. (74).

This heuristic derivation is also supported by the standard perturbation theory. Here we are interested in obtaining the transition probability from some initial state $|m\rangle$ to some other state under the action of a perturbing potential V. The Hamiltonian is characterized by

$$\begin{aligned} H &= H_0 + V, \\ H_0|m\rangle &= E_m|m\rangle, \\ \langle m|H|j\rangle &= \langle m|V|j\rangle \quad (m \neq j), \\ &= \langle m|H_0|j\rangle \quad (m = j). \end{aligned} \tag{77}$$

The probability of decay from state $|m\rangle$ can be shown to be given by

$$Q(t) = 1 - P(t)$$

$$= \frac{1}{\hbar^2}\int_{-\infty}^{\infty} |\langle m|V|k\rangle|^2\, \rho_k \frac{\sin^2(\omega_{km}t/2)}{(\omega_{km}t/2)^2}\, dE_k, \tag{78}$$

where ρ_k is the density of the state and $\hbar\omega_{km} = E_k - E_m$. The standard argument is that the major contribution to the integral comes from the final states k whose energy E_k is close to E_m. This assumption which is valid asymptotically (that is for larger times), implies the standard result

$$Q(t) = (2\pi\rho_k/\hbar)|\langle m|V|k\rangle|^2, \tag{79}$$

based on the formula

$$\int_{-\infty}^{\infty} \frac{\sin^2 z}{z^2}\, dz = \pi. \tag{80}$$

However, for very short times, this argument fails, and indeed

$$Q(t) = \frac{t^2}{\hbar^2}\left(\int_{-\infty}^{\infty} |\langle m|V|k\rangle|^2 \rho_k\, dE_k\right), \tag{81}$$

as can be seen from the fact that $\sin(x) \sim x$ for $x \ll 1$.

The second aspect of the Zeno effect is the notion of wavefunction collapse. Suppose a measurement is made of an observable with an associated operator $\hat{O}$ having the eigenvalues λ_m corresponding to eigenfunction $|\phi_m\rangle$. If the wavefunction before the measurement is $|\Psi\rangle$, then

$$|\Psi\rangle = \sum_m C_m |\psi_m\rangle, \tag{82}$$

where

$$\begin{aligned} \hat{O}|\phi_m\rangle &= \lambda_m|\phi_m\rangle, \\ C_m &= \langle\phi_m|\Psi\rangle, \end{aligned} \tag{83}$$

and the probability of obtaining the value λ_m is $C_m^* C_m$. If the value λ_m is actually obtained, the von Neumann theory of measurement says that immediately after the observation, the wavefunction collapses to the state $|\phi_m\rangle$.

The Zeno effect is difficult to observe in spontaneous decay because the interval in which the decay probability grows quadratically (as t^2) is much shorter than the time required to make measurements. Thus, deviation from the exponential decays for very short and very long times, has not been observed experimentally so far. However, quantum Zeno effect also applies to the inhibition of induced transitions by frequent measurements and can be observed experimentally.

Observation of quantum Zeno effect

A proposal for demonstrating the Zeno effect on an induced transition was suggested by Cook[37]. The principle of this experiment is as follows. Consider a trapped ion with the level structure shown in Figure 17, similar to that used for the observation of quantum jumps. Here level $|3\rangle$ is the ground state, level $|2\rangle$ is an excited metastable state and spontaneous decay from level $|2\rangle$ to $|3\rangle$ is assumed to be negligible. If the ion is in level $|3\rangle$ at time $t = 0$, and a perturbation having the resonance frequency $\omega = (E_3 - E_2)/\hbar$ is applied, a coherent superposition state is created. Let P_2 and P_3 be the probabilities for the ion to be in levels $|2\rangle$ and $|3\rangle$, then

$$P_2(t) = \sin^2(\Omega t/2),$$

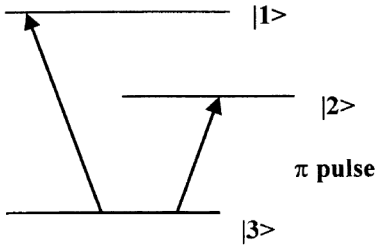

Figure 17. Schematic diagram for the observation of quantum Zeno effect – the proposed scheme.

$$P_3(t) = \cos^2(\Omega t/2), \tag{84}$$

where Ω is the Rabi frequency.

If a measurement of the state of the ion is made after a short time, such that $\Omega t \ll 1$, then $P_3(t) \approx 1$ and $P_2(t) \approx (1/4)\Omega^2 t^2 \ll 1$. If instead, the ion starts out in level $|2\rangle$, the situation is reversed, so that $P_2(t) \approx 1$ and $P_3(t) \approx (1/4)\Omega^2 t^2$.

Assume now that the level $|1\rangle$ is connected by a strongly allowed transition to level $|3\rangle$ and that it can decay only to level $|3\rangle$, the state measurement is carried out by the $|3\rangle \rightarrow |1\rangle$ transition with an optical pulse. This pulse causes a collapse of the wavefunction. The wavefunction of the ion is projected by the measurement into level $|3\rangle$ or $|2\rangle$ with probabilities equal to the square of the wavefunction's amplitude for being in the level $|2\rangle$ or $|3\rangle$. If the ion is projected into level $|3\rangle$ at the beginning of the pulse, it cycles between level $|3\rangle$ and $|1\rangle$ and emits a series of photons until the pulse is turned off. If it is projected into level $|2\rangle$, it scatters no photons.

The idea is to drive the transition $|3\rangle \rightarrow |2\rangle$ with an on-resonance π-pulse of duration $T = \pi/\Omega$, while simultaneously applying a series of short measurement pulses. The duration of the measurement is assumed to be much less than the time between the pulses. Suppose the ion is in the level $|3\rangle$ at $t = 0$. The π-pulse is then applied. Without the measurement pulses, the probability $P_2(t)$ of the ion to be in state $|2\rangle$ is unity. Let n measurement pulses be applied at time $t_k = k(T/n) = k\pi/(n\Omega)$, where $k = 1, 2, \ldots n$. We calculate the probability $P_2(t)$ at the end of the n measurement pulses. For this purpose, we use the optical Bloch equations

$$\frac{\partial \rho_{22}}{\partial t} = i\Omega(\rho_{23} - \rho_{32}) = -\frac{\partial \rho_{33}}{\partial t},$$

$$\frac{\partial \rho_{23}}{\partial t} = i\Omega(\rho_{22} - \rho_{33}). \tag{85}$$

Introducing

$$R_1 = \rho_{23} + \rho_{32},$$
$$R_2 = i(\rho_{23} - \rho_{32}),$$
$$R_3 = \rho_{22} - \rho_{33} = P_2 - P_3, \tag{86}$$

we may write eq. (85) as

$$\frac{dR_1}{dt} = 0,$$

$$\frac{dR_2}{dt} = -2\Omega R_3,$$

$$\frac{dR_3}{dt} = -2\Omega R_2. \tag{87}$$

The above set of equations can be replaced by the precession of the Bloch vector $\vec{R}$

$$\frac{d\vec{R}}{dt} = \vec{\omega} \times \vec{R}, \tag{88}$$

where $\vec{\omega} = (\Omega, 0, 0)$.

If the ion is in the ground state $|3\rangle$ initially ($t = 0$) we have $\vec{R} = (0, 0, -1)$.

Just before the first measurement pulse at $T_1 = \pi/(n\Omega)$, the Bloch vector

$$\vec{R} = (0, \sin \Omega t_1, -\cos \Omega t_1) = (0, \sin(\pi/n), -\cos(\pi/n)). \tag{89}$$

The measurement pulse projects an ion into level $|2\rangle$ or $|3\rangle$. Its effect on the density matrix, which corresponds to an ensemble average, is to set the coherence ρ_{23} and ρ_{32} as zero, while leaving the populations ρ_{22} and ρ_{33} unchanged. That is,

$$\vec{R}_1 = (0, 0, -\cos(\pi/n)). \tag{90}$$

Thus at $t_1 = \pi/(n\Omega)$, just after the first measurement pulse, $\vec{R}$ is the same as it was at $t = 0$, except that its magnitude $|R|$ is decreased by a factor of $\cos(\pi/n)$.

After the second measurement at time $t_2 = 2\pi/(n\Omega)$, $|R|$ is decreased by another factor $\cos(\pi/n)$ due to linearity of the equations of motion. Thus after n measurements, i.e. at $T = \pi/\Omega$ the Bloch vector

$$\vec{R}(t) = (0, 0, -\cos^n(\pi/n)). \tag{91}$$

The required probability $P_2(T)$ follows from the relation

$$P_2(T) = \tfrac{1}{2}[1 + R_3] = \tfrac{1}{2}[1 - (\cos(\pi/n))^n]. \tag{92}$$

For large n,

$$\cos(\pi/n) \approx 1 - \tfrac{1}{2}(\pi/n)^2,$$

$$(\cos(\pi/n))^n \approx \left(1 - \frac{1}{2}\left(\frac{\pi^2}{n}\right)\frac{1}{n}\right)^n \rightarrow e^{-\pi^2/2n}. \tag{93}$$

Thus the probability for induced transition takes the form

$$P_2(t) = \tfrac{1}{2}[1 - e^{-\pi^2/2n}], \tag{94}$$

which tends to zero as $n \rightarrow \infty$.

This experiment was carried out by Wineland's group[38] at NIST using $^9Be^+$ ions confined in a Penning trap and laser-cooled. The effect was observed in an RF transition between two $^9Be^+$ ground state ($2s^2S_{1/2}$) hyperfine levels separated by 320.7 MHz in a magnetic field $B = 0.8194$ Tesla (Figure 18).

Short pulses of light of wavelength 313 nm (which is nearly resonant with sub-level of $2p^2P_{3/2}$ state and indicated by the large double headed arrow in Figure 18), applied at the same time as the RF field was used to make the measurements. The predicted and the observed values of the transition probabilities for $|3\rangle \rightarrow |2\rangle$ and $|2\rangle \rightarrow |3\rangle$ were found to be in good agreement with the theory. The

experiment could be done with a single trapped Hg^+ ion also.

Interaction-free measurement and quantum Zeno effect

In 1962 Dennis Gabor, who invented holography asserted that no observation or measurement can be made with less than a photon, this is true classically, as the interaction-free measurement is a contradiction in classical mechanics. However, by using quantum mechanics some experiments can be devised to achieve interaction-free measurements. A thought-experiment called 'physicist's shell game' is one such experiment containing two shells with a pebble hidden under one of them. The pebble is special in the sense that even if a single photon interacts with it, it will become dust. How do we determine which shell is hiding the pebble? To answer this question, Elitzur and Vaidman[39] devised a thought-experiment to carry out the interaction-free measurement of the pebble. Their experiment consists of an interferometer with two arms having two mirrors and two beam splitters as shown in Figure 19. In this interferometer photon detectors are being used instead of a screen, such that one of the detectors is so positioned that it detects only the equivalent of bright fringes (BRT-D) and the other one records dark fringes (DARK-D), meaning no photon ever reaches here. In this experiment, initially no pebble is present and optics is so arranged that a photon always reaches BRT-D. Next, a pebble is kept in the upper arm (see Figure 19 *b*) of the interferometer. A photon entering at first beam splitter (BS1) has a choice of two paths to follow. Let the photon take the upper arm, then it hits the pebble and destroys it and will not reach the second beam splitter (BS2). If it takes the lower arm, it does not hit the pebble. There will not be any interference occurring at BS2, as the photon has only one way to reach here. At BS2 again there is 50% probability that it can hit BRT-D or DARK-D. Detection of a photon at BRT-D gives no information, because this would have happened in the absence of the pebble also. On the contrary if the photon hits DARK-D then we can say with certainty that there was a pebble in the upper arm, otherwise DARK-D could not have fired. In conclusion, the presence of a pebble in one arm occasionally sends a photon in DARK-D, thus ensuring an interaction-free measurement.

The real experiment using a photon from a nonlinear crystal has been performed[40] to clearly demonstrate that the interaction-free measurement devices can be built. We refer readers to ref. 40 for more details, where the experiment is a slight variation of the Elitzer–Vaidman experiment discussed above.

We now discuss the role of quantum Zeno effect in interaction-free measurement. In 1994, Kasevich (Stanford) proposed an experiment, which was first devised by Ashes Peres (Technion-Israel Institute) in 1980 (see ref. 40 also). The experiment considers the change in pola-

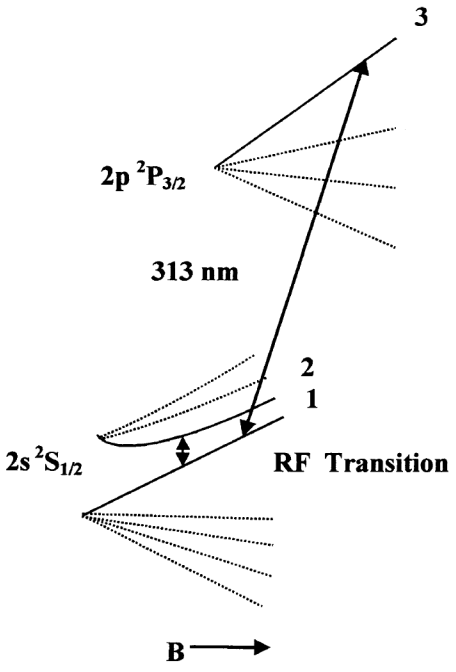

Figure 18. Experimental scheme using $^9Be^+$ ions in a magnetic field.

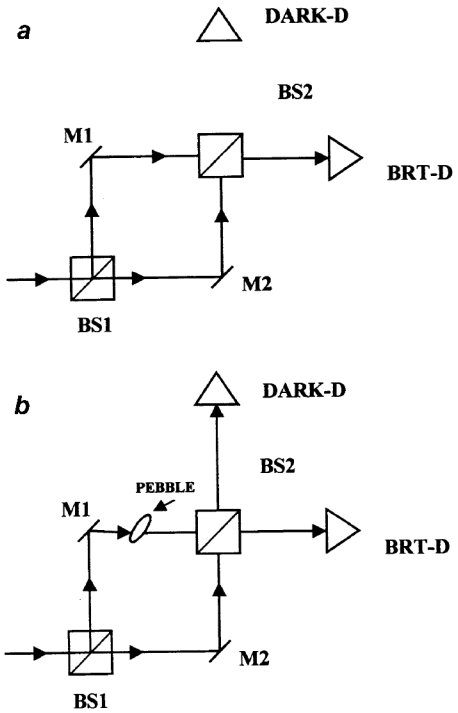

Figure 19. Pebble experiment of Elitzur and Vaidman. In this interferometry experiment a photon can select either of the two paths but the optical elements are so arranged that the photon always goes to BRT-D detector which measures constructive interference (*a*). If a pebble is kept in the upper arm, then the DARK-D occasionally clicks and thus completes the interaction-free measurement (*b*).

rization of light. Polarization means vibration of light wave – it is up and down (side to side) for a vertically (horizontally) polarized light. These vibrations are at right angles to the propagation direction of the light. In this experiment (Figure 20), the light (a single photon) passes through six polarization rotators so that a horizontally polarized light ends up vertically polarized or vice versa. Let the initial photon be horizontally polarized and let each polarization rotator change the polarization by 15°. After passing through six such rotators, the photon polarization will turn by 90° and will become vertically polarized. Thus it will be unable to cross the polarizer which will allow only horizontally polarized photon to pass through. Hence the photon will not be detected by the detector kept behind the polarizer. The quantum evolution in this case is stepwise rotation of polarization, which we want to inhibit. This can be achieved by interspersing horizontal polarizers between any two polarization rotators. The probability of photon absorption in the first horizontal polarizer is $\sin^2(15)$. Suppose the photon survives after the first horizontal polarizer, it will have horizontal polarization only. Again, at the second horizontal polarizer, the probability of photon absorption is $\sin^2(15)$. So, when the photon crosses the sixth horizontal polarizer, its survival probability is $(1 - \sin^2(15))^6 = (\cos^2(15))^6$. Hence, if we have n stages of such polarization rotators and horizontal polarizers, the probability that the photon will survive and strike the detector is given by $(\cos^2(15))^n$. Clearly, when we have $n \to \infty$, the photon will always strike the detector and evolution of the polarization is completely inhibited[40].

The practical apparatus to perform interaction-free measurement (or detecting an object without photon) consists of a hybrid version of the Elitzer–Vaidman apparatus and the Zeno set-up discussed above. The details are as shown in Figure 21. It consists of a fast switchable mirror and the polarization rotator which rotates the photon polarization by 15° in each cycle (in fact an arrangement of mirrors in spiral staircase is used to obtain this[40]). The other part of this apparatus is a polarization interferometer with a polarization beam splitter and two mirrors. The polarization beam splitter used here transmits horizontally polarized light and reflects vertically polarized light. Without the presence of any external object in the arms of the interferometer, the light gets split at the polarizer according to its polarization and reflects back from mirrors, to recombine again at the beam splitter. Thus the emerging light is in the same state as that before it entered, i.e. its polarization rotated by 15° towards the vertical. Hence after six cycles the polarization will be completely vertical for a horizontally polarized light. When an object is placed in the vertical polarization arm, then we come across an interesting situation and even after six cycles, the polarization remains horizontal. This is because now the situation is similar to six polarizers inserted in the quantum Zeno experiment. In the first cycle, the polarization is rotated by 15° from the horizontal so that if the photon is reflected in the vertical polarized arm, then it will be absorbed by the object placed in that arm. The probability for this to happen is 6.7% (= $\sin^2(15)$). If this absorption does not occur, then the photon enters the horizontally polarized arm and its polarization remains horizontal when it returns to the beam splitter. This process is repeated in the six cycles when the bottom mirror is switched off. The result of the measurement shows that the polarization is still horizontal. Thus one can conclude that an opaque object is present in the interferometer. By increasing the number of cycles in the experiments, the photon absorption probability can be made smaller. Experiments conducted at Los Alamos laboratories show that 70% of the measurement could be interaction-free.

Quantum anti-Zeno effect

The Zeno effect in its original sense is related to the spontaneous decay of an unstable state or particle. Normally, spontaneous decay is related to the 'reservoir' of possible states where transition can take place. Recently, Kofman and Kurizki[41] have reopened the issue of dependence of the decay rate on the energy spectrum of the reservoir

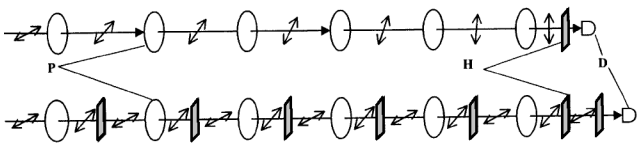

Figure 20. Demonstration of quantum Zeno effect with the help of polarization rotators causing rotation of polarization by 15°. When a horizontally polarized photon crosses six such rotators (P), it becomes vertically polarized (upper row). However, by interspersing a polarizer (H) after each rotator, the photon polarization remained unchanged (lower row).

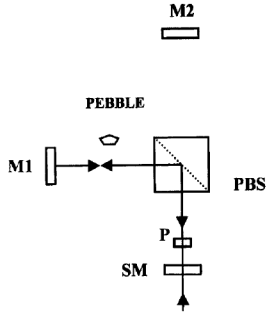

Figure 21. Combined set-up of Elitzur–Vaidman and quantum Zeno effect schemes. Here a photon is entering from below the switchable mirror (SM) and follows the path six times before coming out through the mirror. Polarization of the photon remains horizontal if there is a pebble in one of the paths, otherwise the polarization becomes vertical. P is polarization rotator and PBS is polarization beam splitter.

Box 3. Quantum computing

Components including electrical wires, etc. of a computer can be in two basic states, viz. logical '0' state or logical '1' state depending upon whether no current of some current is flowing through them. A 'bit' of information is represented by either these two states. The process of computation means to logically manipulate bits via logical gates. Instead of logical components, one can use quantized electronic states of atoms designated as ground state $|0\rangle$ and excited state $|1\rangle$, for the purpose of recording information. The generalized state according to the laws of quantum mechanics would be $|\Phi_1\rangle = \alpha|0\rangle + \beta|1\rangle$ (a linear superposition of these two states), and is called a quantum bit or 'qubit'. When there are two qubits, then the general state takes the form $|\Phi_2\rangle = \alpha|00\rangle + \beta|01\rangle + \gamma|10\rangle + \delta|11\rangle$. A special case of this state, when $\alpha = \delta = 0$ and $\beta = \gamma = 1/\sqrt{2}$, is called Einstein–Podolski–Rosen (EPR) state $|\Phi_{EPR}\rangle = (|01\rangle + |10\rangle)/\sqrt{2}$. The degree of correlation of two qubits in $|\Phi_{EPR}\rangle$ is a matter of quantum mechanics, because there is no classical analogue of this state and it is called 'entangled state'. The utilization of entanglement is the basic difference of a quantum computer over its classical counterpart. There is intrinsic parallelism in quantum computing because of this entanglement. The logic used in classical computer is Boolean, but the quantum computer is based on quantum logic.

states and the energy spread of the unstable state. Usually, the 'decay' in a quantum optical system is a consequence of a 'reservoir' of possible states to which transition can occur. Clearly, the decay rate should strongly depend on the spectrum of the reservoir states, as the decay is due to transition to these states. Any measurement means interruption and randomization of the oscillations of the system. If f is the frequency of the sequential measurement, then according to the energy–time uncertainty relation, it will cause an energy spread of $\hbar f$. This energy spread is primarily responsible in determining the range of accessible reservoir states and thus affects the decay rate. The usual quantum Zeno effect should take place when the energy spread due to repeated measurement is much larger compared to the width of the reservoir spectrum (in energy) and the separation in energy between the unstable state and the centre of gravity of distribution of states in the reservoir.

It is more likely that the reverse situation is abundant in natural systems, i.e. the spread of energy due to repeated measurement is much smaller compared to the separation between the unstable state and the nearest maximum in the energy spectrum of the reservoir. Hence the decay becomes faster if the frequency of measurement is increased. Thus the case of anti-Zeno effect occurs as the energy spread of the unstable state increases and correspondingly the accessibility of reservoir states increases and the transition rate becomes faster, and hence the decay is faster with the increase in the frequency of measurement. So, the quantum Zeno effect (QZE) does not hold generally, but only for a restricted class of systems. The QZE is principally unattainable in radiative or radioactive decay because the required measurement rates may cause the system to disintegrate. Acceleration of decay by frequent measurement (the quantum anti-Zeno effect, QAZE) is possible for essentially any decay process and is much more ubiquitous than its inhibition[41]. It has already been noticed that the QAZE is a cause for concern in connection with quantum error correction for quantum computers.

Conclusions and future prospects

We have discussed some non-classical features of light in terms of the correlation functions and the statistics of light along with the experiments to observe these features. The experiments in ion traps discussed here reveal the basic quantum nature of the atom, as pointed out by Bohr. Besides revealing fundamental physics, these experiments provide some unique and ingenious methods for realizing quantum computation. One of the promising methods to realize quantum computation is an ion trap quantum computer. In linear ion traps, AC currents in electrodes generate a time-dependent electric quadrupole field. By suitably adjusting the AC current, it is possible to trap ions of different masses. The linear ion trap has been realized experimentally. It is possible to trap thirty ions[42] in this trap, but so far no quantum computation with thirty ions has been realized. In any quantum computation work, both storage as well as quantum information processing require a lot of experimental ingenuity, because quantum information is fragile. In the case of linear ion trap, the electronic state of ions is used for information storage. The ions are cooled to their ground state of motion so that only the unavoidable motion due to quantum mechanical uncertainty is present. Laser light is utilized to control the electronic transition and hence in manipulating the quantum information. However, the unavoidable interaction of ions with their environment severely limits the power of computation because of decoherence induced by such transitions. To combat this decoherence problem, quantum error corrections are used. Though there is a good theoretical understanding of the various underlying processes in quantum computation, the need of the hour is to realize a fully functional

quantum computer. But despite this, a lot of interesting and fundamental experiments in physics can be carried out with whatever developments have taken place so far.

1. Glauber, R. J., *Phys. Rev.*, 1963, **130**, 2529–2539; **131**, 2766–2788; *Phys. Rev. Lett.*, 1963, **10**, 84–86.
2. Hanbury-Brown, R. and Twiss, R. Q., *Nature*, 1956, **177**, 27–29 and references therein.
3. Pike, E. R., *Quantum Optics* (eds Kay, S. M. and Maitland, A.), Academic Press, New York, 1970.
4. Carmichael, H. J. and Walls, D. F., *J. Phys.*, 1976, **B9**, L43–L46, 1199.
5. Cohen-Tannoudji, C., in *Frontiers in Laser Spectroscopy* (eds Balian, R., Haroche, S., Liberman, S.), North Holland, Amsterdam, 1977.
6. Kimble, H. J., Dagenais, M. and Mandel, L., *Phys. Rev. Lett.*, 1973, **39**, 691–695.
7. Abate, L., *Opt. Commun.*, 1974, **10**, 269–272.
8. Diedrich, F. and Walther, H., *Phys. Rev. Lett.*, 1987, **58**, 203–206.
9. Short, R. and Mandel, L., *Phys. Rev. Lett.*, 1983, **51**, 384–387; Joshi, A. and Lawande, S. V., *J. Mod. Opt.*, 1988, **38**, 135–143; *Phys. Rev.*, 1991, **44**, 716–720; Joshi, A. and Obada, A-S. F., *J. Phys.*, 1997, **30**, 81–97.
10. Walls, D. F., *Nature*, 1983, **306**, 141–146; Slusher, R. E. and Yurke, B., *Sci. Am.*, May 1988, **258**, 32–38, 50–56; Teich, M. C. and Saleh, B. E. A., *Quantum Opt.*, 1989, **1**, 153; Walls, D. F., *Sci. Prog.*, 1990, **74**, 291–310; Kimble, H. J., *Phys. Rep.*, 1992, **219**, 227–234; Fabre, C., *ibid*, 215–225; Dalton, B. J., Ficek, Z and Swain, S., *J. Mod. Opt.*, 1999, **46**, 379–474; Takahashi, H., *Adv. Commun. Syst.*, 1965, **1**, 227; Slusher, R. E., Hollberg, L W., Yurke, B., Mertz, J. C. and Valley, J. F., *Phys. Rev. Lett.*, 1985, **55**, 2409–2412; Kimble, H. J. and Oppo, G. L., *Quantum Dynamics of Simple Systems*, IOP, London, 1996; Polzik, E. S., Carri, J. and Kimble, H. J., *Phys. Rev. Lett.*, 1992, **68**, 3020–3023.
11. Joshi, A. *et al.*, *Phys. Rev.*, **A41**, 1990, 2822–2828; **A43**, 1991, 6428–6431; *Opt. Commun.*, 1991, **86**, 469–474; *J. Mod. Opt.*, **38**, 1991, 2009–2022; *Phys. Rev.*, **A45**, 1992, 2025–2030; *Opt. Commun.*, **94**, 1992, 362–368; *Int. J. Mod. Phys.*, 1992, **6**, 409–415; 1994, **8**, 121–135; *J Phys.*, 1997, **B30**, L557–L566; *Phys. Rev.*, 1998, **A52**, 4239–4243; Jagatap, B. N. *et al.*, *Phys. Rev.*, 1991, **A43**, 6316–6322; 1991, **A44**, 6030; see also ref. 10.
12. Dehmelt, H. G., *Bull. Am. Phys. Soc.*, 1975, **20**, 60; Wineland, D. J. and Dehmelt, H. G., *ibid*, 637.
13. Cook, R. J. and Kimble, H. J., *Phys. Rev. Lett.*, 1985, **54**, 1023.
14. Nagourney, W., Sandberg, J. and Dehmelt, H., *ibid*, 1986, **56**, 2797–2799.
15. Sauter, T., Neuhauser, W., Blatt, R. and Toschek, P. E., *ibid*, 1986, **57**, 1696–1698.
16. Bergquist, J. C., Hulet, R. G., Itano, W. M. and Wineland, D. J., *ibid*, 1986, **57**, 1699–1702.
17. Itano, W. M., Bergquist, J. C. and Wineland, D. J., *Phys. Rev.*, 1988, **A38**, 559–562; Itano, W. M., Bergquist, J. C., Hulet, R. G. and Wineland, D. J., *Physica Scr.*, 1988, **T22**, 79.
18. Hulet, R. G., Wineland, D. J., Bergquist, J. C. and Itano, W. M., *Phys. Rev.*, 1988, **A37**, 4544–4547; Hulet, R. G. and Wineland, D. J., *ibid*, 1987, **A36**, 2758–2762.
19. Cirac, J. I. and Zoller, P., *Phys. Rev. Lett.*, 1995, **74**, 4091–4094.
20. Hughes, R. J. *et al.*, *Fortschr. Phys.*, 1998, **46**, 329.
21. Sauter, T., Blatt, R., Neuhauser, W. and Toschek, P. E., *Opt. Commun.*, 1986, **60**, 287–292; Blatt, R. and Zoller, P., *Eur. J. Phys.*, 1988, **9**, 250–256.
22. Block, M., Rehm, O., Seibert, P. and Werth, G., *Eur. Phys. J.*, 1999, **D7**, 461–465.
23. Stacey, D. N., Barton, P. A., Donald, C. J. S., Lucas, D. M., Stevens, D. A. and Steane, A. M., 2000, arXive:physics/0002026; Stacey, D. N. *et al.*, 2000, arXive:physics/0003085.
24. Mollow, B. R., *Phys. Rev.*, 1969, **188**, 1975.
25. Dalibard, J., Castin, Y. and Molmer, K., *Phys. Rev. Lett.*, 1992, **68**, 580–583; Carmichael, H. J., *An Open System Approach to Quantum Optics*, Springer, Berlin, 1993.
26. Javanainen, J., *Phys. Rev.*, 1986, **A33**, 2121–2123.
27. Schenzle, A., DeVoe, R. G. and Brewer, R. G., *ibid*, 2127–2130.
28. Schenzle, A. and Brewer, R. G., *ibid*, 1986, **A34**, 3127–3142.
29. Kimble, H. J., Cook, R. J. and Wells, A. L., *ibid*, 1986, **A34**, 3190–3195.
30. Cohen-Tannoudji, C. and Dalibard, J., *Europhys. Lett.*, 1986, **1**, 441–448.
31. Zoller, P., Marte, M. and Walls, D. F., *Phys. Rev.*, 1987, **A35**, 198–207.
32. Kim, M. S., Knight, P. L. and Wodkiewicz, K., *Opt. Commm.*, 1987, **62**, 385–388; Kim, M. S. and Knight, P. L., *Phys. Rev.*, 1987, **A36**, 5265–5270.
33. Nienhuis, G., *ibid*, 1987, **A35**, 4639–4649.
34. Pegg, D. T., Loudon, R. and Knight, P. L., *ibid*, 1986, **A33**, 4085–4091.
35. Agarwal, G. S., Lawande, S. V. and D'Souza, R., *Phys. Rev.*, 1988, **A37**, 444–449; Lawande, Q. V., Joshi, A. and Lawande, S. V., *J. Phys.*, 1995, **A28**, 5903–5917; Lawande, S. V., in *Developments in Theoretical Physics* (eds Ray, S. M., Sahni, V. C. and Burma, M.), Oxford and IBH, New Delhi, 1988, p. 192; Lawande, S. V. and Joshi, A., *Phys. News*, 1991, **22**, 64–74.
36. Misra, B. and Sudershan, E. C. G., *J. Math. Phys.*, 1977, **18**, 756–763; Chiu, C. B., Sudershan, E. C. G. and Misra, B., *Phys. Rev.*, 1977, **D16**, 520–529.
37. Cook, R. J., *Phys. Scr.*, 1988, **T21**, 49.
38. Wineland, D. J., Itano, W. M., Heinzen, D. J. and Bollinger, J. J., *Phys. Rev.*, 1990, **A41**, 2295–2300.
39. Elitzur, A. C. and Vaidman, L., *Found. Phys.*, 1993, **23**, 987.
40. Kwiat, P. G., Weinfurter, H., Herzog, T., Zeilinger, A. and Kasevich, M. A., *Phys. Rev. Lett.*, 1995, **74**, 4763–4766; Kwiat, P. G., Weinfurter, H. and Zeilinger, A., *Sci. Am.*, Nov. 1996, 52–58.
41. Kofman, A. G. and Kurizki, G., *Phys. Rev.*, 1996, **A54**, R3750–R3753; *Nature*, 2000, **405**, 546–550.
42. Waki, I., Kassener, S., Birkl, G. and Walther, H., *Phys. Rev. Lett.*, 1992, **68**, 2007–2010.

ACKNOWLEDGEMENTS. We thank Prof. Howard Carmichael, Prof. Surendra Singh, Prof. H. J. Kimble, Prof. H. Walther and Dr John Vaccaro for many helpful discussions. We also thank our colleagues Prof. R. K. Bullough, Prof. G. S. Agarwal, Dr Q. V. Lawande and Dr R. D'Souza for their support. One of us (S.V.L.) would like to thank CSIR for generous financial support.

Received 27 July 2001; revised accepted 14 February 2002